

Prototyping a Novel Core Loss Tester for Assembled Stator
Lamination Stacks

Jaydeep Bhalala

A Thesis

in

The Department

of

Electrical and Computer Engineering

Presented in Partial Fulfillment of the Requirements

for the Degree of Master of Applied Science (Electrical Engineering) at

Concordia University

Montréal, Québec, Canada

April 2020

© Jaydeep Bhalala, 2020

**CONCORDIA UNIVERSITY
SCHOOL OF GRADUATE STUDIES**

This is to certify that the thesis prepared

By: Jaydeep Bhalala

Entitled: Prototyping a Novel Core Loss Tester for Assembled Stator Lamination Stacks

and submitted in partial fulfillment of the requirements for the degree of

Master of Applied Science (Electrical and Computer Engineering)

complies with the regulations of this University and meets the accepted standards with respect to originality and quality.

Signed by the final examining committee:

| | |
|-------------------------|-------------------|
| _____ | Chair |
| Dr. L.A.C. Lopes | |
| _____ | External Examiner |
| Dr. M. Ghafouri (CIISE) | |
| _____ | Internal Examiner |
| Dr. L.A.C. Lopes | |
| _____ | Supervisor |
| Dr. P. Pillay | |

Approved by: _____
Dr. Y.R. Shayan, Chair
Department of Electrical and Computer Engineering

_____ 20 _____

_____ Dr. Amir Asif, Dean,
Faculty of Engineering and Computer
Science

ABSTRACT

Prototyping a Novel Core Loss Tester for Assembled Stator Lamination Stacks

Jaydeep Bhalala

In the modern industrial world, electrical machines have become the backbone of the industry. Electrical machines account for nearly 60% of the total electricity consumption in the industrialized countries, hence a huge energy saving can be achieved even by a small increment in electrical machine efficiency. This improvement starts right at the machine design stage. Improving the machine design requires accurate quantification of the machine losses. A significant portion of the losses in the electrical machines is due to the core loss in the magnetic material. The core loss measurement in the stators and rotors is still an open problem. Most of the available techniques and testers for core loss estimation do not take into account the effect of the various mechanical processes and shape of the magnetic material under test. In addition, most of the current standardized core loss estimation techniques and testers are based on pulsating magnetic field only, whereas all the rotating electrical machines have a rotational magnetic field.

In this research work, a new core loss tester to measure core loss in assembled stator lamination stacks is analysed, simulated and prototyped with successful result validation between simulation and experimental tests. The new tester is suitable for the measurement of rotational core loss, and is capable of measuring loss with different number of pole combinations and excitation frequencies. Measurements were carried out using an induction machine stator.

This work describes the influence of different flux patterns generated based on the number of poles in the excitation winding. Experimental tests were carried out and the core loss data were recorded for various test cases. The developed tester accounts for the effect of mechanical processes like punching, laser cutting, stack pressing, etc. Experimental results are obtained from the tester are compared with the simulated results and the percentage difference in the core loss is presented. The core losses measured by the standardized pulsating core loss testers like Epstein frame are compared with that measured from the new tester to study the

effect of rotational excitation on the core loss measurement. This work also presents the shortcomings of using commercially available pulsating loss data for core loss simulation by comparing the simulated results with the experimentally measured core loss.

Acknowledgements

No one achieves anything alone! MASc is a journey and the reason I could reach it's destination was due to the help, guidance, motivation and unwavering support of several wonderful people throughout.

First of all I would like to thank Lord Swaminarayan, Brahm Swarup Pramukhswami Maharaj and Guruhari Mahantswami Maharaj for inspiring me everyday to do something great, for providing gift of life, energy and zeal they provided from beginning, through it all, till the end and for the future to come.

I would like to thank my parents and my elder brother. Their cheer up during each course completion and research achievements constantly fueled in the encouragement and inspiration to me. Besides that, it was the source of motivation to produce best out of myself.

Prof. Pillay gave me an opportunity to pursue my MASc under his supervision for which I will always be grateful to him. Apart from his technical guidance throughout my MASc, I have also learned from him that "Just because it's hard doesn't mean it can't be done", a valuable lesson I will carry forward. I am also grateful for the financial support and confidence he instilled in me during this program. I would like to take this opportunity to thank him for all his teachings and financial aid to pursue this program.

I have a lot of respect and appreciation towards all my MASc committee members, Prof. Lopes and Prof. Ghafouri. Their questions during the oral examination significantly helped me to improve understanding of my work.

I would also thank all my friends in the peer group. Being the junior most among all of my colleagues was a great experience for me. I have learned a great deal from them, having had the opportunity to interact with several of them. Special thanks to Dr. Maged Ibrahim for the guidance during the design phase of my work and Dr. Christophe for all the help with 3-D CAD drawings. Thanks to Dr. Mathews, Dr. Chirag, Dr. Amit, Dr. Mahmood, Dr. Masadeh, Rajendra, Dwaipayan, Sumeet, Mohan, Bigyan, Tamanwe, YuPeng and Gayatri (and several others whom I might have missed here). You made my stay at PEER Lab memorable and knowledgeable.

Last but not the least a special thanks goes to my roommates and friends who supported me in my good and bad times and took care of me like a brother. Thank you so much Radhey, Shyam, Anand, Karshan, Kirtan and Yogesh.

This research work is done as part of NSERC/Hydro-Quebec Senior Industrial Research Chair entitled Design and Performance of Special Electrical Machines held by Professor Pragasen Pillay at Concordia University. I would like to acknowledge the support of the Natural Sciences & Engineering Research Council of Canada.

Finally, I would like to dedicate my MSc to my parents. I know my parents are brimming with pride wherever they are. Their pride is what I have been striving for during my entire academic career.

Contents

| | |
|--|------|
| List of Figures | ix |
| List of Tables..... | xiii |
| 1. Introduction | 1 |
| 1.1 The Need of Core Loss Estimation | 1 |
| 1.2 Review of Core Loss Estimation Methods..... | 1 |
| 1.2.1 Pulsating Core Loss Measurement | 2 |
| 1.2.2 Rotational Core Loss Measurement | 5 |
| 1.3 Thesis Objective..... | 8 |
| 1.4 Contributions..... | 8 |
| 1.5 Thesis Outline | 9 |
| 2. Analysis of a New Core Loss Tester | 10 |
| 2.1 Introduction..... | 10 |
| 2.2 Need of New Core Loss Tester | 10 |
| 2.3 Stator Core Loss Tester Analysis..... | 13 |
| 2.3.1 Stator Core Loss Tester Principle | 13 |
| 2.3.2 Design of the Analyzed Tester | 13 |
| 2.4 Initial Simulation Results..... | 16 |
| 2.4.1 Simulation Results for Different Number of Poles | 16 |
| 2.4.2 Simulation Results with Sinusoidal and Non-Sinusoidal Excitation | 17 |
| 2.5 3-D FEA Simulation Results..... | 18 |
| 2.5.1 Development of 3-D FEA Simulation..... | 18 |
| 2.6 Analytical Core Loss Calculation | 20 |
| 2.7 Summary | 22 |
| 3. Theory, Development and Construction of New Core Loss Tester | 24 |
| 3.1 New Core Loss Tester Structure | 24 |
| 3.1.1 Tester Core..... | 24 |
| 3.1.2 Excitation Coils..... | 25 |
| 3.1.3 Sensor Coils | 26 |
| 3.2 Development of the Tester | 28 |
| 3.3 Tester Setup..... | 31 |
| 3.4 Experimental Setup..... | 32 |
| 3.5 Working of the New Tester..... | 34 |
| 3.6 Testing, Calibration and Loss Separation Procedure | 35 |

| | |
|---|----|
| 3.7 Summary | 36 |
| 4. Experimental Results and Comparison with FEA Simulation Results..... | 37 |
| 4.1 Tester Calibration using Ring Tester | 37 |
| 4.2 Tester to Stator Flux Density Ratio Calibration..... | 38 |
| 4.3 Experimental Results | 40 |
| 4.3.1 Signals Obtained from the Stator and the Tester Sensor Coils | 41 |
| 4.3.2 Core Losses Measured Under Influence of Rotational Magnetization | 43 |
| 4.4 Comparison of Experimental Results, FE Simulation and Analytical Calculation..... | 49 |
| 4.5 Summary | 50 |
| 5. Conclusions and Future Work | 52 |
| 5.1 Conclusions | 52 |
| 5.2 Limitations | 53 |
| 5.3 Future Work | 54 |
| 5.4 Applications | 54 |
| References | 56 |
| Appendix | 60 |

List of Figures

| | |
|---|----|
| Figure 1.1: 700-Turn Epstein frame..... | 2 |
| Figure 1.2: 280-Turn Epstein frame..... | 3 |
| Figure 1.3: Toroid tester..... | 4 |
| Figure 1.4: Single sheet tester..... | 4 |
| Figure 1.5 : Rotational single sheet tester for different sample shape (a) Square (b) Hexagonal | 6 |
| Figure 1.6: 16-pole Halbach Round Single sheet tester..... | 7 |
| Figure 1.7: 24 Slots Induction Machine Round Single sheet tester..... | 7 |
| Figure 2.1: Stator core loss estimation by winding coils on stator stack under test | 10 |
| Figure 2.2: Stator stack core loss tester with C-shape magnetizing coil..... | 11 |
| Figure 2.3: C-shaped core loss tester [24]..... | 12 |
| Figure 2.4: C-shaped coil tester for stator core loss estimation [27] | 12 |
| Figure 2.5: Analyzed core loss tester core and toroidal winding of tester..... | 13 |
| Figure 2.6: Tester winding connection for (a) 2-pole, (b) 4-pole and (c) 6-pole configuration | 14 |
| Figure 2.7: Final geometry of the tester (dimensions in mm)..... | 15 |
| Figure 2.8: FEA simulated flux for: (a) 2-pole, (b) 4-pole and (c) 6-pole..... | 15 |
| Figure 2.9: FEA simulated flux density distribution for (a) 2-pole, (b) 4-pole and (c) 6-pole | 16 |
| Figure 2.10: FEA simulated air gap flux density distribution for winding connections with different pole arcs | 17 |
| Figure 2.11: Comparison between the FEA simulated air gap flux density waveform in a surface permanent magnet motor and the corresponding waveform generated by the tester.. | 17 |
| Figure 2.12: FEA simulated flux density contour plot of the tester and the stator with 4-pole connection of excitation winding and excited with 2-phase, 100 Hz, 15 A peak current waveform | 18 |
| Figure 2.13: The instantaneous induced emf sensed by the tester slot pick-up coils in FE simulation with 4-pole tester connection | 19 |
| Figure 2.14: The instantaneous values of back iron flux density with 4-pole tester connection in FE simulation..... | 19 |
| Figure 2.15: The instantaneous induced emf sensed by the tester tooth pick-up coils in FE simulation with 4-pole tester connection | 20 |

| | |
|--|----|
| Figure 2.16: The instantaneous values of the tester tooth flux density with 4-pole tester connection in FE simulation | 20 |
| Figure 2.17: Core loss calculation algorithm used for core loss estimation for the new tester and stator [26] | 21 |
| Figure 3.1: The Tester Core (a) 3-D design of the tester core (b) The tester core made up of non-oriented silicon steel during winding process..... | 24 |
| Figure 3.2: The excitation coils in 3-D CAD model..... | 25 |
| Figure 3.3: The excitation coil during winding process..... | 25 |
| Figure 3.4: The concept of a search coil or pick-up coil technique: V - voltage induced in the coil, N - number of turns in the coil, A - area enclosed by the coil, B - flux density..... | 26 |
| Figure 3.5: Slot pick-up coil and Tooth pick-up coil in 3-D CAD diagram | 27 |
| Figure 3.6: (a) Insulation paper to insulate winding from the tester in slot (b) Insulating tube to insulate the winding in the inner portion on the tester..... | 28 |
| Figure 3.7: CAD diagram of the tester winding (a) Excitation coil (b) Tooth pick-up coil (c) Slot pick-up coil..... | 29 |
| Figure 3.8: The tester core and winding coils (a) Excitation coil (b) Sensor coil (c) Insulating sleeve (d) End-winding spacer..... | 29 |
| Figure 3.9: Tester windings during the winding process | 30 |
| Figure 3.10: The tester with completed winding | 30 |
| Figure 3.11: The tester with (a) Glue filled slots to insulate excitation coils from the top edge of the slots (b) Excitation coil end-connections separated from each other with insulation paper | 31 |
| Figure 3.12: Tester setup (a) Excitation coil terminals (b) Slot pick-up coil terminals (c) Tooth pick-up coil terminals (d) Tester (e) Terminal box..... | 32 |
| Figure 3.13: The tester setup (a) Cooling fan (b) Winding coil leads..... | 32 |
| Figure 3.14: The experimental setup block diagram..... | 33 |
| Figure 3.15: The experimental setup (1) Computer (2) dSPACE® DS1103 controller (3) Power amplifier (4) Power meters (5) Voltage/current isolation (6) Tester setup with stator under test (7) Thermometer and thermocouples..... | 34 |
| Figure 3.16: Ring tester for the tester calibration | 36 |
| Figure 4.1: Specific core loss of the tester measured using the ring test according to the ASTM A927 standard..... | 37 |
| Figure 4.2: Tester to stator back iron flux density ratio for 2-pole connection at various frequencies | 39 |

| | |
|---|----|
| Figure 4.3: Tester to stator back iron flux density ratio for 4-pole connection at various frequencies | 39 |
| Figure 4.4: Tester to stator back iron flux density ratio for 6-pole connection at various frequencies | 40 |
| Figure 4.5: The stator and the tester CAD diagram with dimension in mm | 40 |
| Figure 4.6: The instantaneous output voltage signals at 100 Hz and 4-pole winding connection in the tester sensor coils (slot pick-up coils) | 41 |
| Figure 4.7: The instantaneous values of the magnetic flux density at 100 Hz and 4-pole winding connection in the tester constructed by integrating the instantaneous voltage waveforms of the tester sensor coils (slot pick-up coils) | 41 |
| Figure 4.8: The instantaneous output voltage signal at 100 Hz and 4-pole winding connection in the tester tooth sensor coils (tooth pick-up coils) | 42 |
| Figure 4.9: The instantaneous output voltage signal at 100 Hz and 4-pole winding connection in the stator back iron sensor coils (stator slot pick-up coils) during the tester to stator flux density ratio calibration..... | 42 |
| Figure 4.10: The instantaneous values of the magnetic flux density at 100 Hz and 4-pole winding connection in the stator constructed by integrating the instantaneous voltage waveforms of the stator sensor coils (stator slot pick-up coils)..... | 43 |
| Figure 4.11: Specific core loss of the stator under test measured with the new core loss tester with 2-pole connection of the excitation coil winding..... | 44 |
| Figure 4.12: Specific core loss of the stator under test measured with the new core loss tester with 4-pole connection of the excitation coil winding..... | 44 |
| Figure 4.13: Specific core loss of the stator under test measured with the new core loss tester with 6-pole connection of the excitation coil winding..... | 45 |
| Figure 4.14: Specific core loss of the stator under test measured with the new core loss tester with 2-pole, 4-pole and 6-pole connection of the excitation coil winding at 60 Hz and 100 Hz frequency..... | 46 |
| Figure 4.15: Specific core loss of the stator under test measured with the new core loss tester with 2-pole, 4-pole and 6-pole connection of the excitation coil winding at 200 Hz and 400 Hz frequency..... | 46 |
| Figure 4.16: Comparison of the specific core loss of the stator measured with the new tester with 2-pole connection and the Epstein frame at 60 Hz, 100 Hz, 200 Hz and 400 Hz | 47 |
| Figure 4.17: Comparison of the specific core loss of the stator measured with the new tester with 4-pole connection and the Epstein frame at 60 Hz, 100 Hz, 200 Hz and 400 Hz | 47 |

Figure 4.18: Comparison of the specific core loss of the stator measured with the new tester with 6-pole connection and the Epstein frame at 60 Hz, 100 Hz, 200 Hz and 400 Hz48

List of Tables

| | |
|--|----|
| Table 2.1: Comparison of simulated and calculated core loss | 22 |
| Table 3.1: Excitation coil winding specifications | 26 |
| Table 3.2: Slot and tooth pick-up coil winding specifications..... | 27 |
| Table 4.1: Core loss comparison between the new tester and the Epstein frame | 49 |
| Table 4.2: Core loss comparison among FE simulation, analytical calculation and experimental results | 50 |

1. Introduction

1.1 The Need of Core Loss Estimation

Energy efficiency has become a major global concern with the rapid growth of worldwide energy consumption. Electrical machines consume a majority of the electricity generated around the globe. Electric motor drive systems used 68 % of the total electricity generated in the United States during the year 2013 [1]. Therefore, improving the efficiency of electric machines has become a research area of significant interest in the past few decades. Improvements in the design aspects of the electrical machines have resulted in better efficiency. The losses in electrical machines are generally divided into four groups: conductor losses (copper losses), core losses (iron losses), mechanical losses (friction and windage losses) and stray losses. A better understanding of these loss components allows researchers to analyze and reduce the losses. Several methods have been developed and implemented in order to reduce the dominant core losses and improve the machine efficiency. The dynamic behaviour of core losses, limited measurement techniques and non-uniform flux density make the analysis challenging in electrical machines.

Core losses in the electrical machines constitutes a significant portion of the total losses ranging from 15 - 25 % in small and medium induction machines operating with sinusoidal supplies [2]. Moreover, they are among the highest in MW rated machines, which uses a large amount of steel. For example, 45 % of the total loss in large synchronous motors used in cement and mining industry is accounted by core losses [3]. Permanent magnet (PM), switched reluctance (SR) and induction machines operated with pulse width modulation (PWM) converters make core loss analysis difficult due to the non-sinusoidal flux waveforms [4]. This also results in higher specific core losses compared to the machines operated with sinusoidal supplies. The core losses are frequency and flux density dependent quantity. Therefore, they are important for the design of high power density and high-speed machines, mostly being used in the defence and the aerospace industry, where operating frequency ranges from 400 Hz to 1.5 kHz. These high power density machines are also employed in electrical transportation [5].

1.2 Review of Core Loss Estimation Methods

Characterization of the soft magnetic materials used in manufacturing of electrical machines is done by placing them in magnetic field. The core losses and relative permeability

are determined at a particular frequency and flux density. There are two types of magnetizers or testers used for the characterization pulsating and rotational.

1.2.1 Pulsating Core Loss Measurement

The pulsating magnetizers generate unidirectional fields. They are similar to a single phase transformer. The sample under test, forms part of the core. The magnetizing current and induced magnetic voltage in the secondary winding gives the value of magnetic field and flux density respectively. The core losses are obtained from the B-H loop area or by the watt-metric method. In the pulsating case, the magnitude of the B-vector varies with time but direction always remains the same.

There are three test fixtures, which can be used for the pulsating core loss measurements: 1) Single sheet tester, 2) Epstein frame and 3) Toroid tester. These testers have been standardized by the American Society of Testing and Material (ASTM) [6] [7] [8] [9]. Pulsating core losses are usually measured by using the watt-metric method due to the simplicity of the measurement technique and the easy availability of the apparatus. This method is also known as voltmeter-ammeter-wattmeter method.

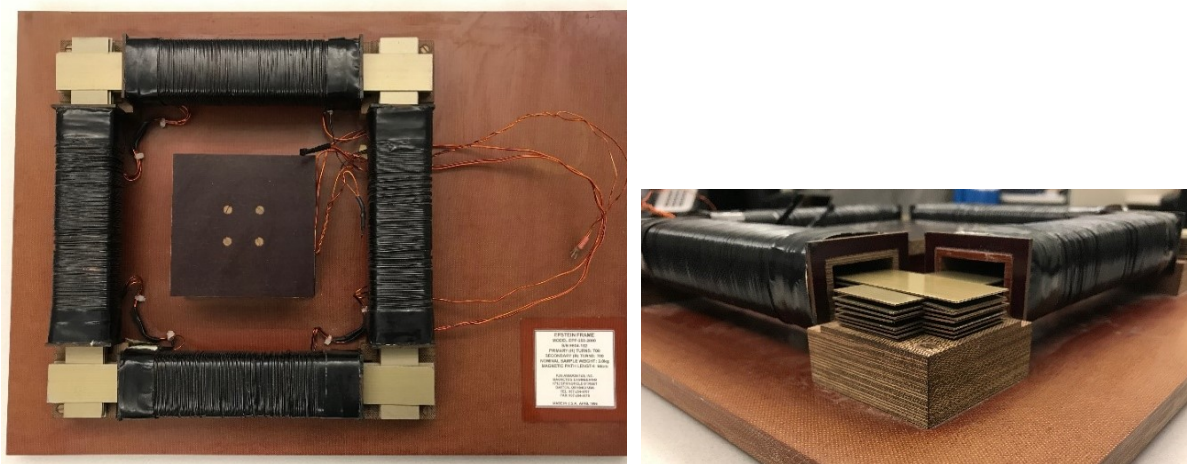


Figure 1.1: 700-Turn Epstein frame

1.2.1.1 Epstein Frame

The Epstein frame is the most widely used method for magnetic testing. It is simple to setup and offers good representation of the magnetic properties of the material under test. Most of the core loss and relative permeability data are measured using an Epstein frame. The Epstein frames are usually classified based on the number of turns, 700, 352 and 280-turns

frames are common. Figure 1.1 shows a 700-turns Epstein frame and Figure 1.2 shows a 280-turn Epstein frame.

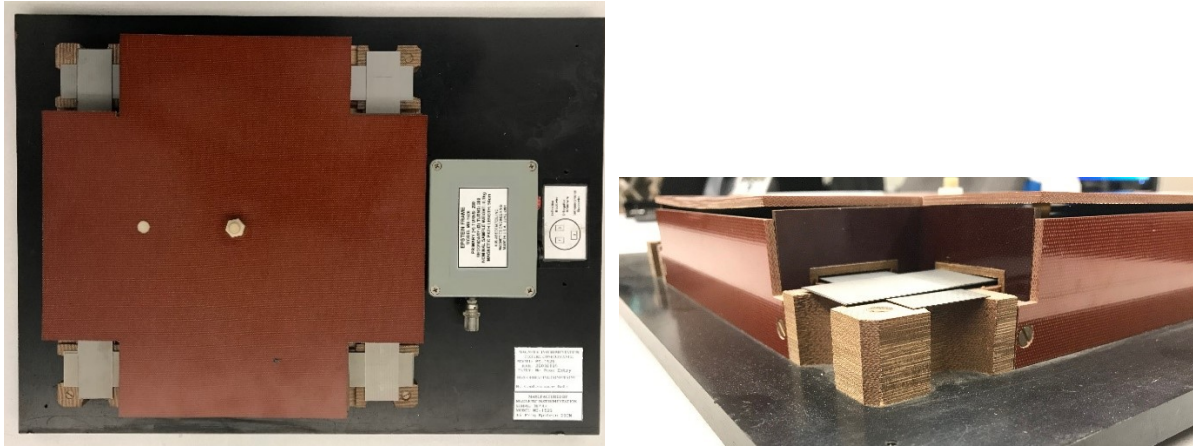


Figure 1.2: 280-Turn Epstein frame

The 700-turns frame is used for low frequency measurements up to 4 kHz. The 280 turn frame is capable of reaching high flux density at frequency up to 6 kHz. The standard size, material preparation and testing conditions are listed in standard ASTM A343 [6]. However, an Epstein frame has its own errors, the leakage flux around the joints and the assumption of 94 cm effective magnetic path length results in errors in the measurements.

1.2.1.2 Toroid Tester

Toroids can produce circular flux paths similar to actual flux distribution in radial flux electrical machines and therefore, are preferred by machine designers. In addition, a toroid forms a closed magnetic circuit, which results in the reduction of the magnetic reluctance. Figure 1.3 shows a Toroid tester. The longer preparation time for toroids make them less desirable. The secondary B-coil is always wound inside in the toroid assembly in order to make the cross section area of the sample under test and the B-coil equal. The primary H-coil is wound over the B-coil. The material preparation and testing conditions are listed in the standard ASTM A927 [8].

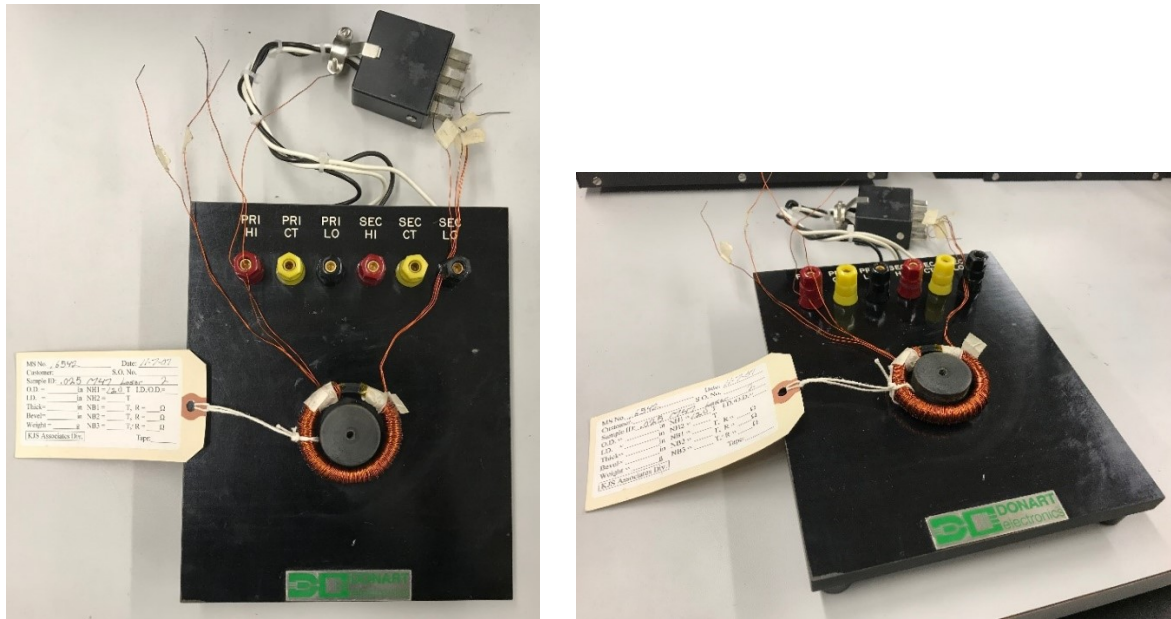


Figure 1.3: Toroid tester

1.2.1.3 Single Sheet Tester

The single sheet tester is the simplest among the three testers. The sample preparation is also very easy and cost effective since it requires only one Epstein strip for testing. However, as the flux is only measured at the centre of the sample strips, measurements obtained from a single sheet tester have the same errors as in the case of an Epstein frame tester. The single sheet tester shown in Figure 1.4 is designed according to ASTM 804 [9]. Due to the limitation of temperature monitoring, it is capable of performing measurements only from 20 Hz to 400 Hz. A major limitation of this tester is that it requires results from an Epstein frame and toroid tester for calibration [10].

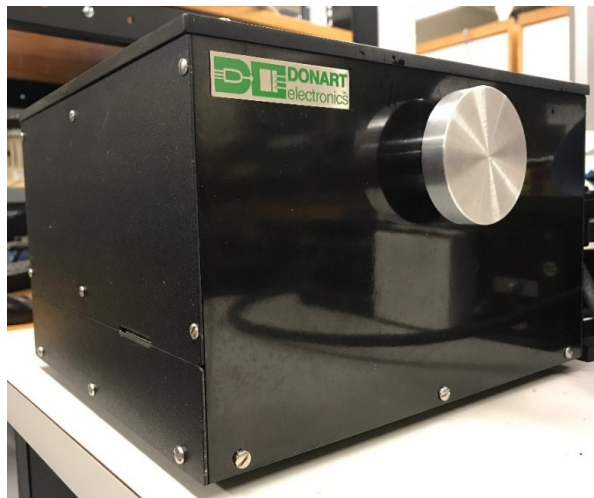


Figure 1.4: Single sheet tester

1.2.2 Rotational Core Loss Measurement

There is lot of work going on to standardize the rotational core loss measurement procedure and test fixtures [11]. For accurate estimation and modeling of core losses in rotational electrical machines and transformer with T – joints, along with pulsating core loss data, rotational core loss data is also required. Most of the work in core loss estimation has been done with pulsating data only, such as models available in Finite Element Analysis (FEA) packages. Manufacturers usually provide core loss data at a frequency of 50/60 Hz and up to a flux density of 1.5 T. Accurate core loss estimation is important since the high speed and the high power machines (MW rated) are required to work beyond this frequency and flux density. In addition, hotspot detection in core is very important in high power density machines to avoid the failure of the core.

There are three commonly used methods for the rotational core loss measurement: torque-metric, thermo-metric and field-metric. The torque-metric method can measure the core losses at high flux densities but it is rarely used due to the complex set up. The thermo-metric method measures the core losses as heat dissipated from the sample under test. The core losses in the material are associated with the change in the core temperature due to the change in the applied field. The disadvantage of the thermo-metric method is that the position of the temperature sensor can alter the material properties and affect the field distribution. The limitations of the thermo-metric method are slow response and inability to measure the core losses at low flux densities due to the negligible thermal response [12] [13]. In field-metric method, the area of the B-H loop is calculated to obtain the core losses. The main advantage of field-metric method is the ability to measure the core losses for wide range of flux density (0.1 T – 2 T). However, the accuracy is dependent on the proper sensor alignment, sensor accuracy, sensitivity, proper analysis of the measured field and field uniformity in the sample measured area. Misalignment of the sensor will result in a significant error between the losses measured with clockwise (CW) and anticlockwise (ACW) rotational magnetization [14].

Field-metric method is used in the design of the following magnetizers for rotational core loss measurement: square single sheet tester (SSST), Halbach round single sheet tester (HaRSST), conventionally wound induction machine round single sheet tester (CW-IMRSST) and sinusoidally wound induction machine round single sheet tester.

1.2.2.1 Rotational Single Sheet Tester (RSST)

The rotational single sheet testers (RSST) are classified according to the sample shape: square, hexagonal and circular. A square magnetizer of 80 mm by 80 mm sample size, with an air-gap of 2 mm and a measurement area of 20 mm by 20 mm is considered in [15]. The SSST is useful in the analysis of the flux density variation due to the effect of the sample shape and the concentrated winding. A pair of orthogonal coils generates the field in the SSST. It has a large number of turns and simple design and can achieve moderately high flux density. A SSST is shown in Figure 1.5(a). The major drawback of the SSST is that, due to leakage flux it is difficult to achieve high and uniform flux density at the centre of the sample in the interpolar regions [15]. Figure 1.5(b) shows a hexagonal RSST [16].

1.2.2.2 Halbach Rotational Single Sheet Tester (HaRSST)

Round single sheet testers are more useful due to their uniform magnetization in most of the magnetization direction. An electromagnetic Halbach RSST with 200 mm sample diameter, 10 mm frame depth and 16 poles from [17] is shown in Figure 1.6. The highest non-uniformity in flux density is dependent on the alignment of the direction of magnetization with the slot opening in a HaRSST. By varying the yoke depth, the number of poles and the sample diameter, the magnetic loading can be increased with acceptable uniformity [16].

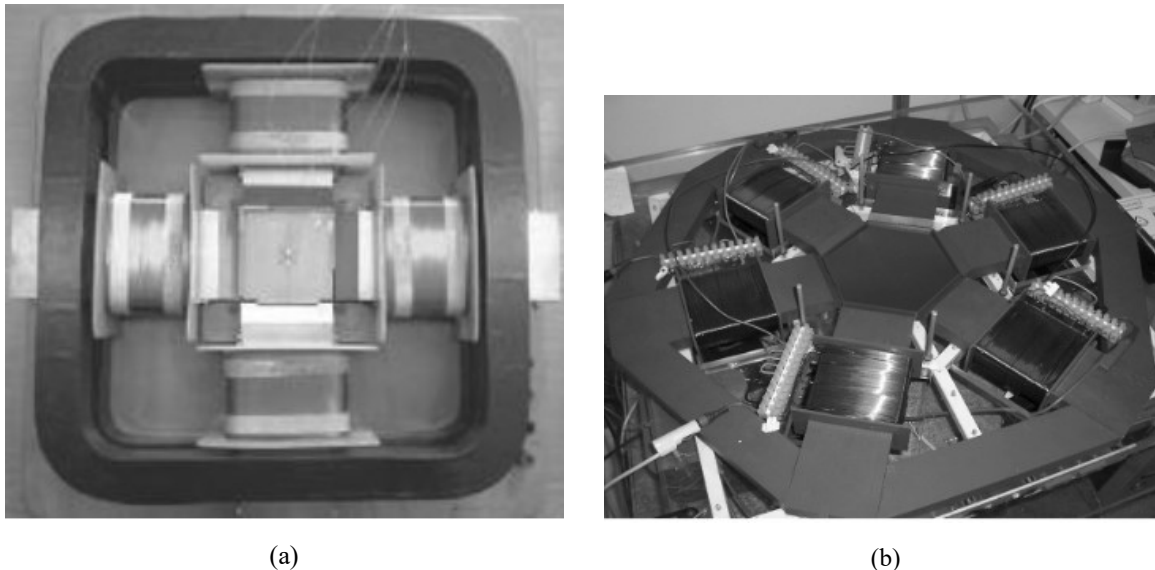


Figure 1.5 : Rotational single sheet tester for different sample shape (a) Square (b) Hexagonal

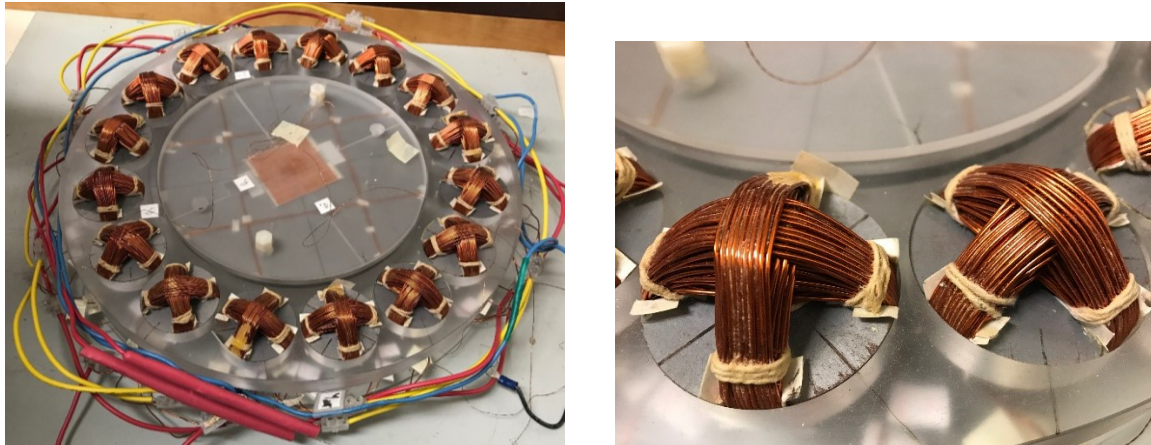


Figure 1.6: 16-pole Halbach Round Single sheet tester

1.2.2.3 Conventionally Wound IMRSST

The conventionally wound IMRSST (CW-IMRSST) has a conventional winding on the chosen induction machine stator core with an inner diameter of 109 mm with 36 slots and 4 poles. To improve the uniformity of the mmf distribution, the quotient of the number of slots and the number of poles must be an integer. Conventional winding results in the variation of the flux density with different magnetization direction.

1.2.2.4 Sinusoidally Wound IMRSST

Sinusoidal distribution of winding results in the uniform distribution of mmf in all the magnetizing direction. This greatly reduces the variation in the flux density in the magnetizer as compared to all other magnetizers. A sinusoidally wound IMRSST with 2 phases, 24 slots, 90 mm inner diameter and 80 mm yoke depth from [16] is shown in Figure 1.7.



Figure 1.7: 24 Slots Induction Machine Round Single sheet tester

1.3 Thesis Objective

The objectives of this thesis are:

- To prototype a novel core loss tester for core loss estimation in assembled stator cores prior to final motor assembly.
- To investigate the effect of the manufacturing process like laser cutting, punching and stack pressing on the magnetic properties of the soft magnetic materials.
- To better understand the behaviour of the soft magnetic material under the influence of rotational magnetization.
- To compare the results obtained from the analyzed tester against the standard pulsating core loss measurement techniques like the Epstein frame.

1.4 Contributions

The contributions of this research work are summarized below.

- Prototype of new core loss tester for core loss estimation in assembled stator lamination stacks
- Application of watt-metric method for rotational core loss estimation
- Improved understanding of rotational core loss in rotating electrical machines
- Improved understanding of effect of excitation frequency and number of poles on rotational core loss estimation
- Analysis of effect of mechanical processes performed during stator manufacturing on magnetic properties and core loss of soft magnetic materials

Conference Papers

1. **J. Bhalala** and P. Pillay, “Prototyping a Novel Core Loss Tester for Assembled Stator Lamination Stacks,” *2020 IEEE Energy Conversion Congress and Exposition (ECCE)*, Detroit, MI, USA, 2020. – **In review**
2. M. Ibrahim, **J. Bhalala** and P. Pillay, “Design of a Core loss Tester for the Evaluation of Assembled Stator Cores of Electric Machines,” *2020 IEEE Energy Conversion Congress and Exposition (ECCE)*, Detroit, MI, USA, 2020. – **In review**

1.5 Thesis Outline

The thesis is divided into five chapters. Chapter two presents the design procedure and design details along with the Finite Element simulation and the primary simulation results to prove the working of the analyzed tester. Chapter three presents the development, constructional details, the theory of the working of the analyzed tester and the testing and calibration procedure for the new tester. In chapter four, the analyzed tester is tested by varying the number of poles and frequency and the results are compared with the simulation results and standard pulsating core loss measurement techniques. Chapter five concludes the thesis, outlines the limitations and provides suggestions for the future work.

2. Analysis of a New Core Loss Tester

2.1 Introduction

There is a growing demand for high efficiency electric machines, especially for the applications that require effective utilization of a limited stored energy, such as Electric Vehicles (EVs) and Hybrid Electric Vehicles (HEVs). On the other hand, machine designers are faced with a challenge to reduce the machine losses without increasing the size, weight and cost. The core loss in an electrical machine accounts for a significant portion of the total loss at high speed-low torque condition, which is common in a highway drive cycle of EVs and HEVs [18]. One of the most promising approaches for improving the efficiency of the electric machines is to reduce the core loss in the machine steel core. This can be achieved by using high-grade steels and optimizing the steel core design.

2.2 Need of New Core Loss Tester

Core losses in electrical machines are usually calculated in the post processing stage of Finite Element Analysis (FEA) based simulation using the Epstein frame data provided by steel manufacturers [7] as explained in Chapter 1. However, the manufacturing processes such as punching, laser cutting, stacking and shrink fit, etc., deteriorate the steel magnetic properties and increase its core losses [19] [20] [21] [22]. Therefore, it is essential to develop a test method for measuring the core losses in the steel cores of electrical machines after the lamination core assembly.

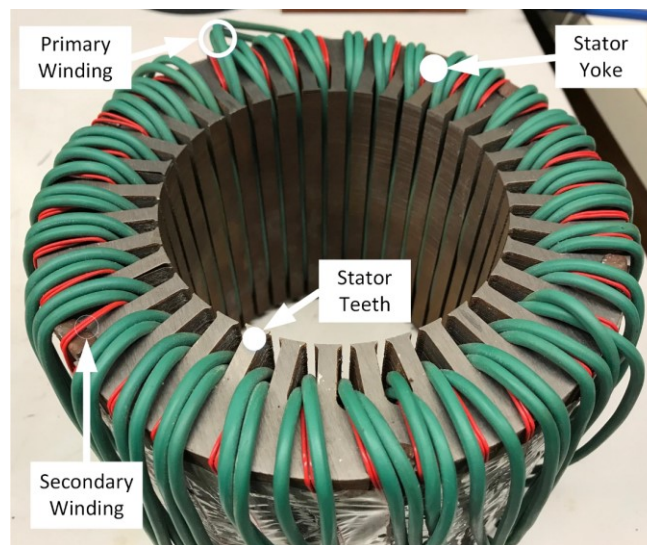


Figure 2.1: Stator core loss estimation by winding coils on stator stack under test

Several methods are reported to assess the degradation of magnetic properties in the fabricated stator cores [23] [24] [25] [26]. Technically, it is still a challenge to realize both high and uniform magnetic flux density within a wide area of the electrical steel stack under test. The magnetic properties of the steel cores can be measured using the test system shown in Figure 2.1, where the primary and secondary windings are wrapped around the stator yoke into the slots in order to generate an alternating flux circulating around the stator yoke. However, this method only measures the core losses in the stator yoke, and the core losses in the teeth are not evaluated. In addition, for this method, the primary and secondary coils have to be wound for each tested stator core. This is not practical for evaluating the core losses for a large number of stator cores.

In [24] and [27], the analysis of flux density distribution in the stator stack shows that the main flux is concentrated in a certain part of the stack under test due to the non-uniform excitation by C or H shaped magnetizing coils as shown in Figure 2.2 and Figure 2.3. Therefore, the measured losses by this tester do not account for the anisotropic effects caused by the steel rolling direction. Therefore, several measurements have to be performed at different angles in order to average the steel anisotropic effects. In addition, the generated flux in the steel core is entirely alternating flux, which differs from the actual flux in the rotating AC machine, which has rotating flux components at the tips and roots of the stator teeth [28]. Therefore, this tester will not be able to measure the effect of rotational magnetisation on assembled stator core. Due to this, the importance is given to developing test fixtures, which are capable of performing 2-D rotating field tests.

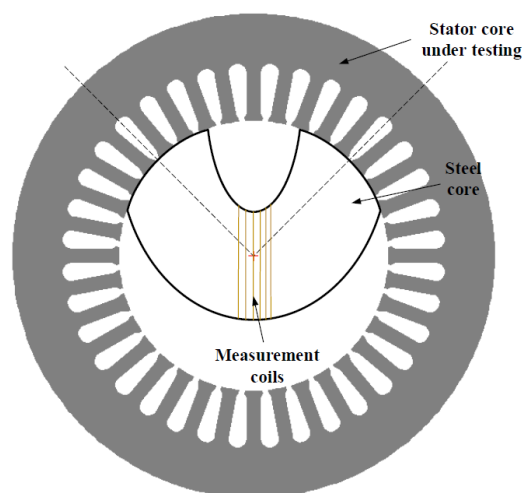


Figure 2.2: Stator stack core loss tester with C-shape magnetizing coil

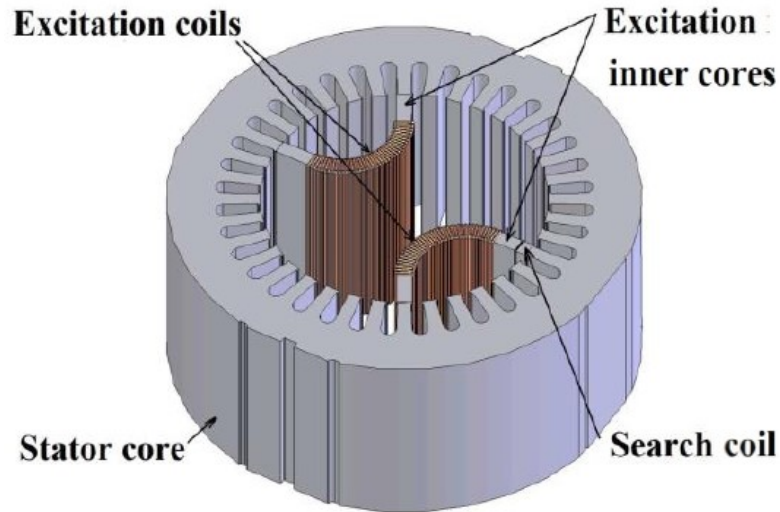


Figure 2.3: C-shaped core loss tester [24]

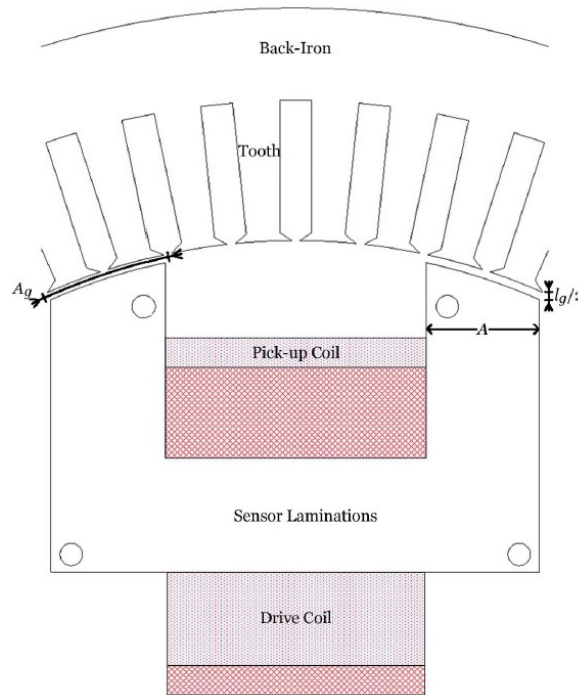


Figure 2.4: C-shaped coil tester for stator core loss estimation [27]

In this chapter, a new core loss tester is analyzed to emulate the actual flux experienced in the stator of a rotating AC machine. Dr. Maged Ibrahim proposed this new concept during his stay at Concordia University as a Postdoctoral Researcher under guidance of Prof. Pillay. A new concept based on the assembled stator core loss tester is analyzed to produce rotating fields with controlled number of poles, spatial distribution and excitation waveforms in the stator under test. Extensive simulations are performed using FEA to study the magnetic field distribution in the stator stack compared to the previous designs.

2.3 Stator Core Loss Tester Analysis

2.3.1 Stator Core Loss Tester Principle

The analyzed core loss tester is similar to the stator of an AC machine with an outer rotor. The tester employs toroidal windings that are wrapped around the back iron as shown in Figure 2.5. The coils in each slot are accessible at the tester terminal in order to allow flexibility in changing the number of poles. When the tester is excited using two-phase AC currents, it produces a rotating flux in the stator core under test with a number of poles that depends on the winding connection. The stator core under test serves as the return path for the flux and the flux pattern will be same as in the case of a radial flux rotating electrical machine. Therefore, it will produce the same effect of running a radial flux electrical machine on the stator of the electrical machine. The design proposed by Dr. Maged has the capability to produce rotating fields with a controlled number of poles, spatial distribution and excitation waveforms and therefore, it can emulate the actual fields occurring in different electric machine types with different design variations as discussed in the following sections.

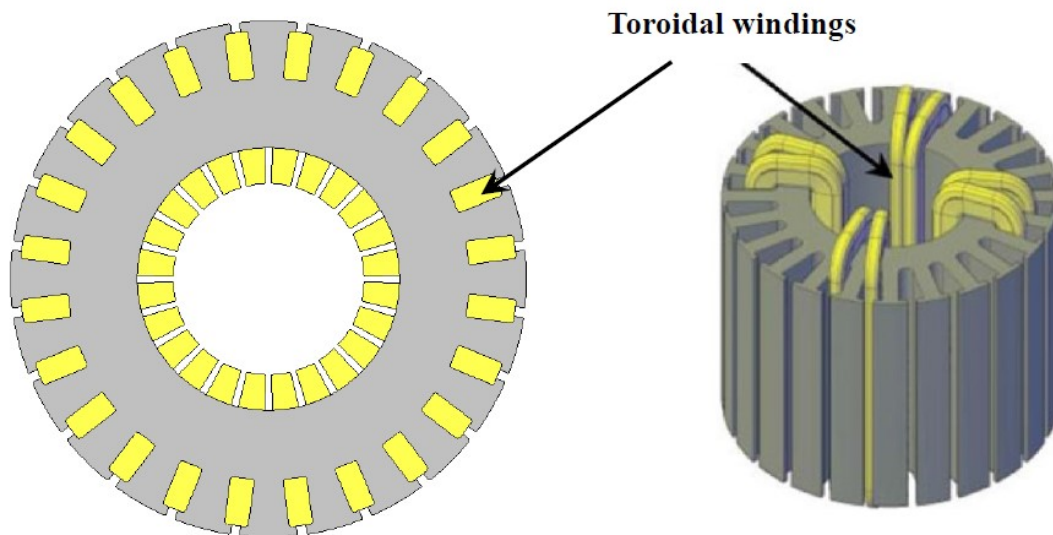


Figure 2.5: Analyzed core loss tester core and toroidal winding of tester

2.3.2 Design of the Analyzed Tester

Dr. Maged Ibrahim proposed the initial design of the new tester. A magnetizer was designed to induce a time-dependent magnetic flux with controlled magnitude and frequency in the teeth and yoke of the stator under test. The coils in each slot are accessible at the tester terminal in order to allow flexibility in changing the number of poles as shown in Figure 2.6.

The tester is expected to be able to induce a large enough flux such that the flux density in certain areas of the stator stack under test should be able to reach saturation of the material's B-H characteristics. Some of the important design considerations to achieve this are given below:

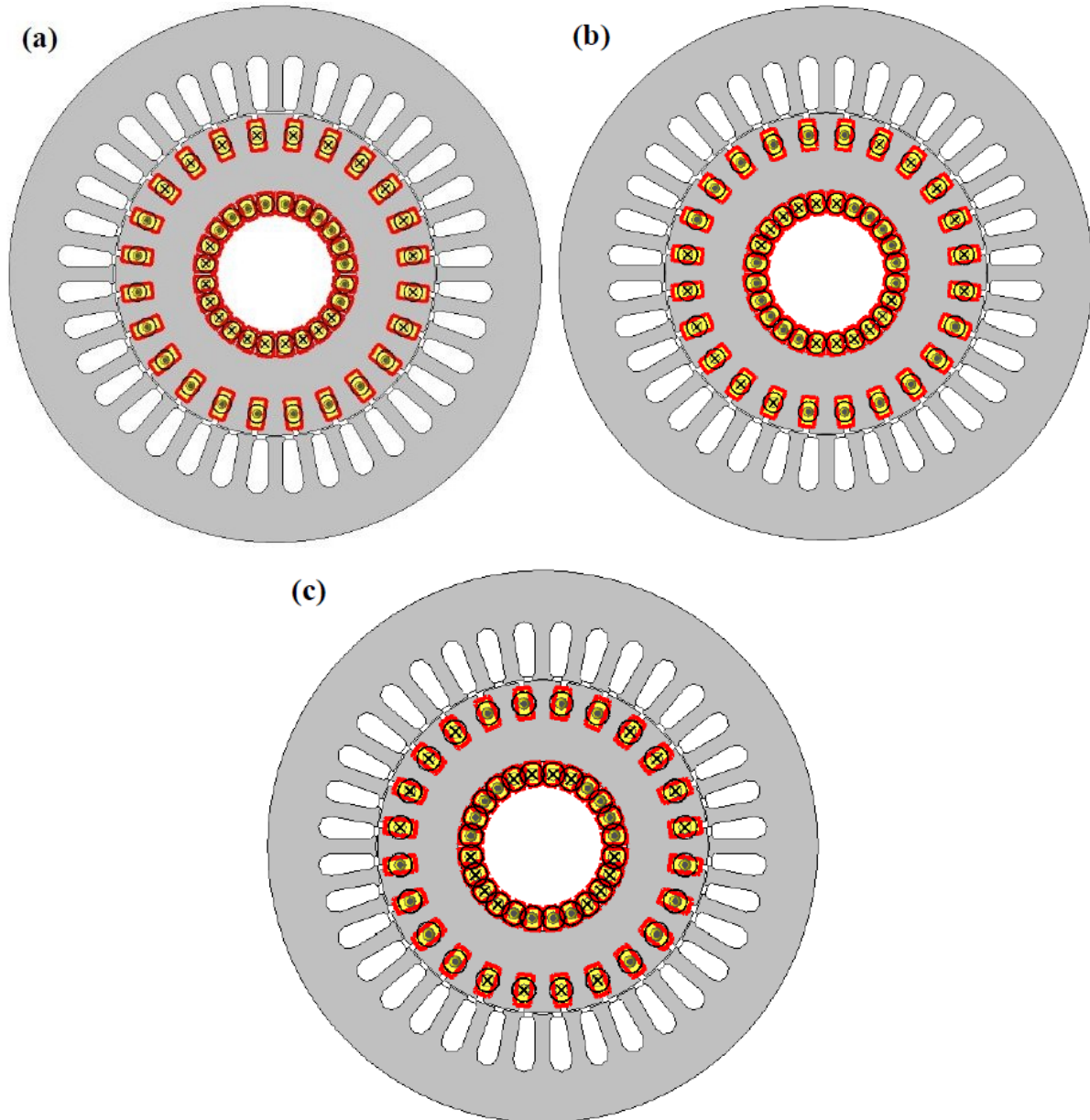


Figure 2.6: Tester winding connection for (a) 2-pole, (b) 4-pole and (c) 6-pole configuration

1. The tester outer diameter is dependent on the inner diameter of the stator under test and the air gap. The air gap should not be too large in order to minimize leakage flux from the tester to stator.
2. Optimizing the current density in the excitation coil in order to keep the required number of turns of the coil minimum, thus making slot size as small as possible for required ampere-turns and making the design practical and economical.

3. Large flux density applies a large magnetic field and results in a large number of ampere-turns.
4. The excitation coil was wound using Litz wire (a bundle of individually enameled strands) to minimize the skin effect.

During the initial design process, the core loss tester was simulated using JMAG[®] 2-D FEA along with the stator core of a 5 hp induction motor. A 24-slot configuration is chosen, as it can generate 2-pole, 4-pole and 6-pole rotational fields when excited from two 90° phase-shifted current sources. It is also possible to utilize three-phase excitation to generate 2-pole and 4-pole rotational fields with reduced harmonics. The geometry of the tester is as shown in Figure 2.7. The geometry of the tester is dependent on the slot loading to induce the required ampere-turns and the magnetic flux in the tester and the stator. Figure 2.6(a) shows the winding connection for the 2-pole configuration. Similarly, Figure 2.6(b) and Figure 2.6(c) gives the winding connection for the 4-pole and 6-pole connection respectively.

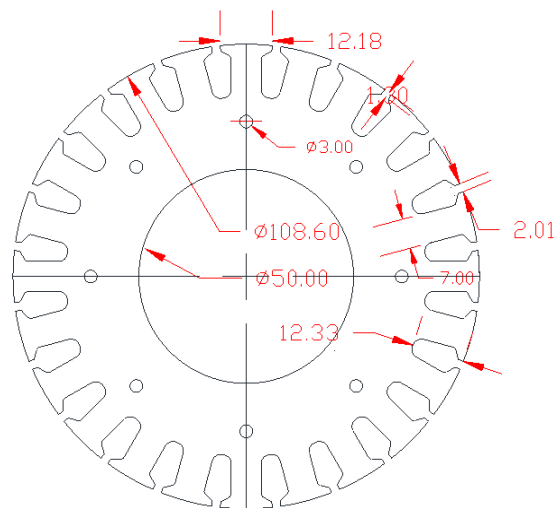


Figure 2.7: Final geometry of the tester (dimensions in mm)

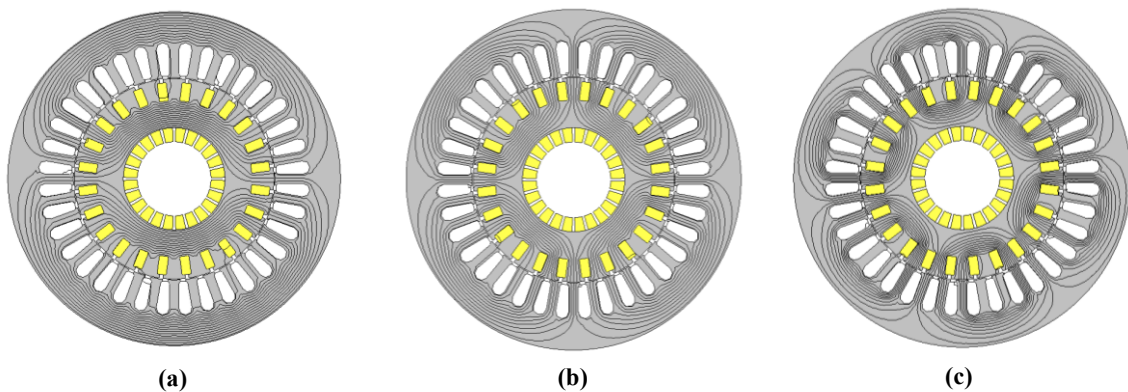


Figure 2.8: FEA simulated flux for: (a) 2-pole, (b) 4-pole and (c) 6-pole

2.4 Initial Simulation Results

2.4.1 Simulation Results for Different Number of Poles

The simulation results show that the tester is capable of producing a rotating flux similar to the one inside rotating AC machines with a number of poles that can be controlled based on the winding connection. Figure 2.8 shows the FEA simulated flux distribution (flux lines) for 2-pole, 4-pole and 6-pole winding connections. Figure 2.9 shows the flux density distribution in the tester and the stator stack with different number of poles. It is clearly evident from Figure 2.9 that the flux density in certain areas of the stator like teeth and back iron reaches the saturation region of the B-H curve of the silicon steel. For the 2-pole connection,

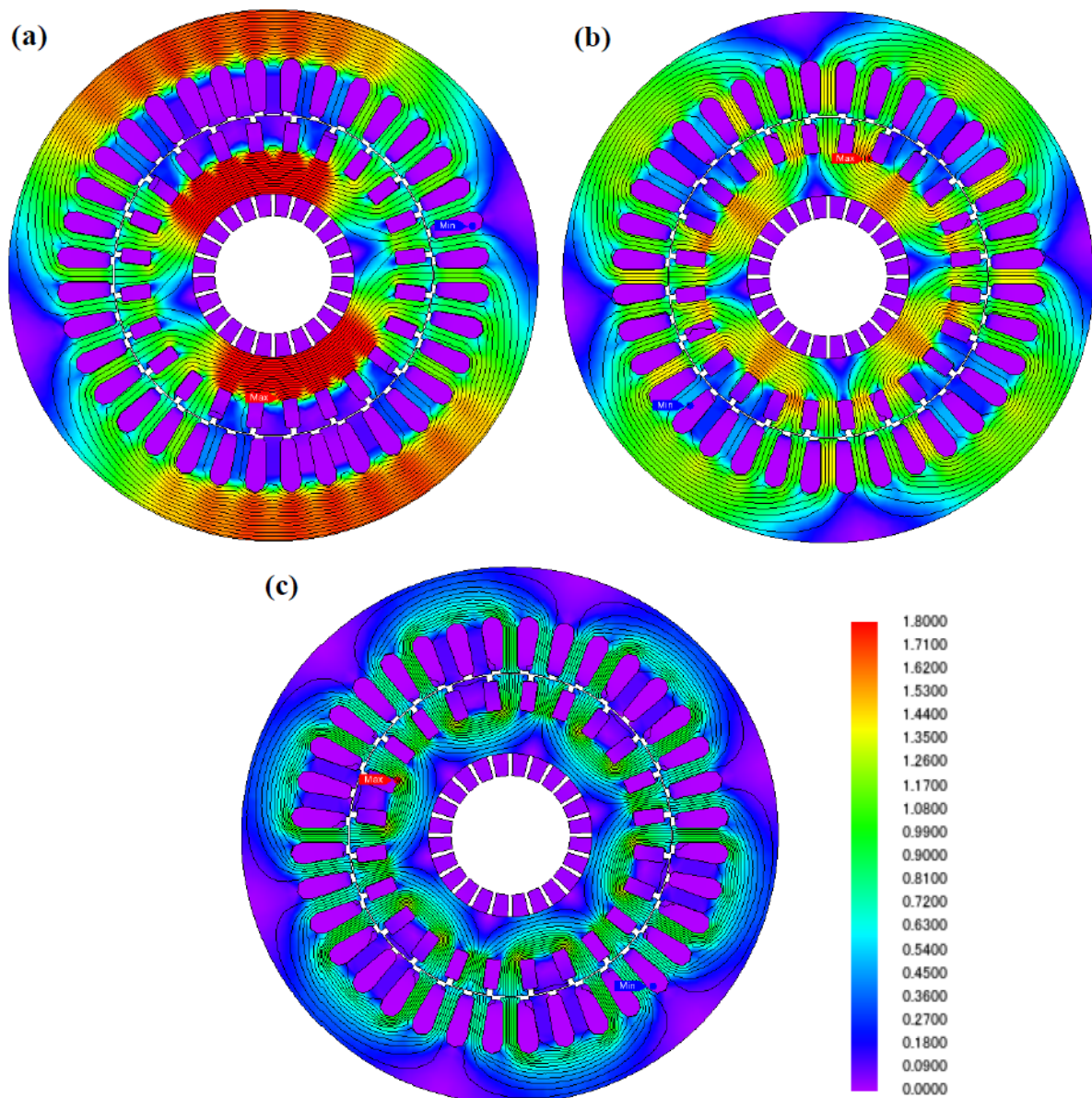


Figure 2.9: FEA simulated flux density distribution for (a) 2-pole, (b) 4-pole and (c) 6-pole

a large portion of stator back iron and some of the teeth experiences flux density as high as 1.65 T as shown in Figure 2.9(a). Similarly, peak flux density values of 1.5 T and 1.25 T is seen in Figure 2.9(b) and Figure 2.9(c) for the 4-pole and 6-pole connections respectively. This proves the ability of the analyzed tester to induce high enough flux density in the stator under test.

2.4.2 Simulation Results with Sinusoidal and Non-Sinusoidal Excitation

The toroidal configuration of the excitation winding allows the windings to be full or short pitched. This can be utilized for the experimental evaluation of the impact of short pitching on the core loss of induction and wound-rotor synchronous machines and utilized to emulate the magnet pole arc variation in the rotor of a Permanent Magnet (PM) AC machine. Figure 2.10 shows the FEA simulation of the spatial distribution of the air gap flux when the windings are short pitched by one, two and three slots. This corresponds to pole arc angles of 45°, 60° and 75°.

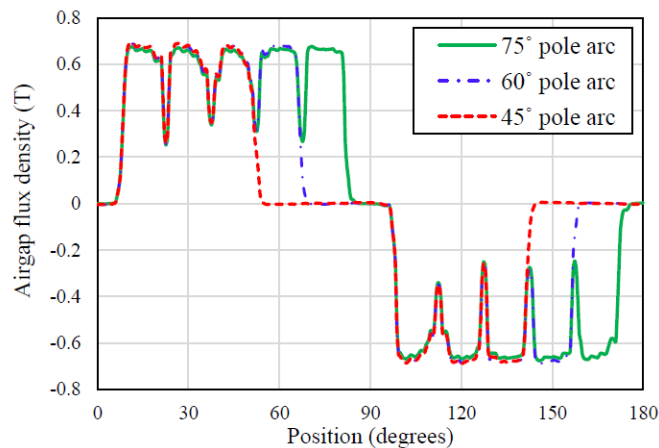


Figure 2.10: FEA simulated air gap flux density distribution for winding connections with different pole arcs

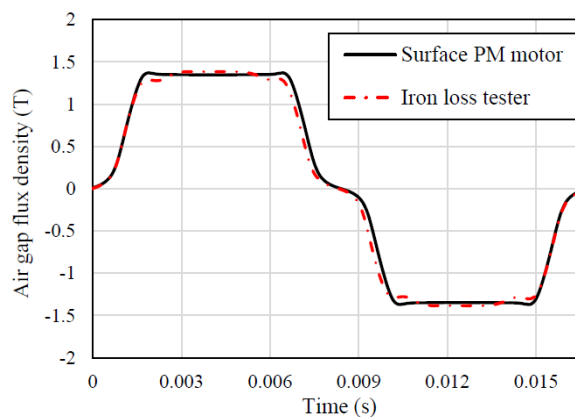


Figure 2.11: Comparison between the FEA simulated air gap flux density waveform in a surface permanent magnet motor and the corresponding waveform generated by the tester

For the evaluation of the stator cores of induction and wound-rotor synchronous machines, the two or three phase windings of the tester should be excited with sinusoidal current waveforms. On the other hand, for PM machines, the flux waveforms tend to have non-sinusoidal variation in time, as shown in FEA simulation results for a surface PM in Figure 2.11. These waveforms can be reproduced by exciting the windings of the core loss tester with the motor FEA simulated flux waveforms and can be seen in Figure 2.11. These simulation results shows the use of tester to test the stator under the influence of non-sinusoidal air gap flux density distribution.

2.5 3-D FEA Simulation Results

2.5.1 Development of 3-D FEA Simulation

The 2-D FEA simulation discussed in the previous section is extended to 3-D FEA simulation along with the inclusion of the tester slot pick-up coils and the tester tooth pick-up coils to obtain the tester back emf and the tester tooth induced emf waveforms along with the flux density.

The FEA simulated flux density contour plot for the 4-pole connection of the excitation winding is given in Figure 2.12. The tester is excited with a 2-phase sinusoidal supply of 100 Hz and 15 A peak current waveform. The flux density distribution in the tester and the stator

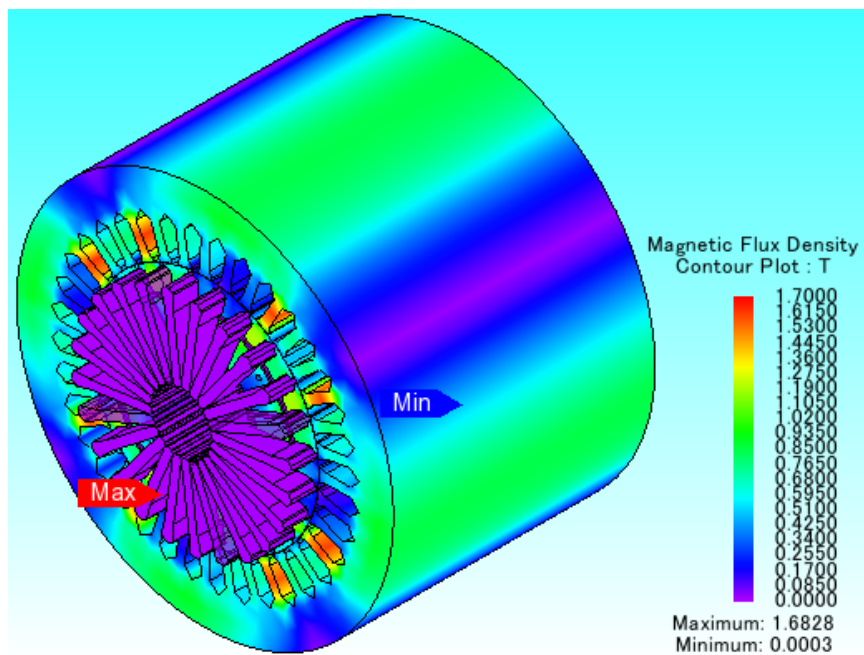


Figure 2.12: FEA simulated flux density contour plot of the tester and the stator with 4-pole connection of excitation winding and excited with 2-phase, 100 Hz, 15 A peak current waveform

is similar to a radial flux electrical machine as can be seen from Figure 2.12. The contour plot also shows that the stator and tester teeth have high flux density. These teeth will have higher core losses, which, may result in a local hot spot, when the machine is operated for a long duration. Therefore, the new tester will help in better understanding these regions with higher core loss compared to rest of the stator and tester.

The tester back iron induced emf in the FE simulation sensed by slot pick-up coils is as shown in Figure 2.13. The distortion in the initial part of the waveform is due to the initial transients in the simulation. Only one cycle of the simulated waveform is presented due to the excessively long simulation run time. The tester was excited with 2-phase, 100 Hz and 15 A peak sinusoidal current waveform. The peak flux density that is observed in the tester back iron in this condition was 1 T. The tester back iron flux density waveforms are shown in Figure 2.14. These waveforms are verified later through experimental results in order to prove that the new core loss tester is working according to the design.

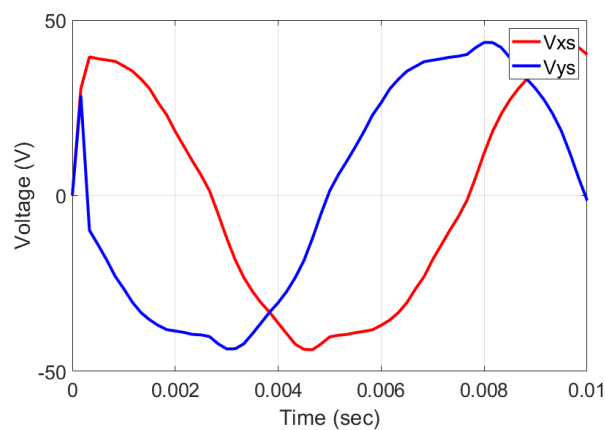


Figure 2.13: The instantaneous induced emf sensed by the tester slot pick-up coils in FE simulation with 4-pole tester connection

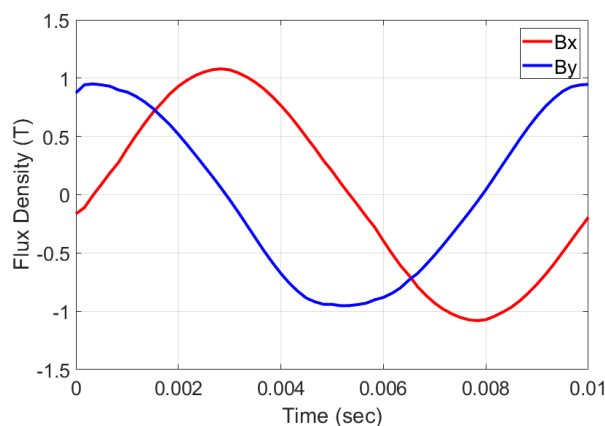


Figure 2.14: The instantaneous values of back iron flux density with 4-pole tester connection in FE simulation

The induced emf in the tester tooth pick-up coil is given in Figure 2.15. Figure 2.16 shows the magnetic flux density in the tester tooth. The tester tooth coils are left individually without any series connection with other tooth coils. All the above waveforms are produced from the data generated during Finite Element simulation using JMAG[®] FE software.

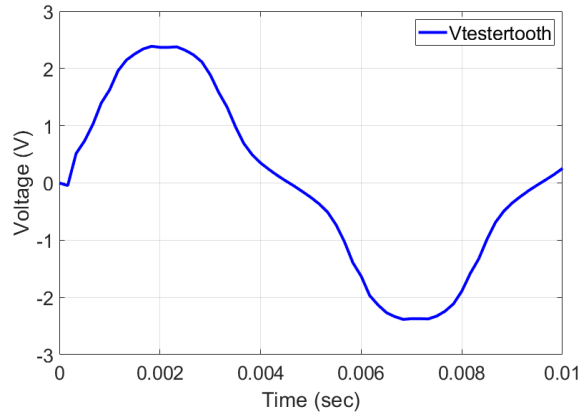


Figure 2.15: The instantaneous induced emf sensed by the tester tooth pick-up coils in FE simulation with 4-pole tester connection

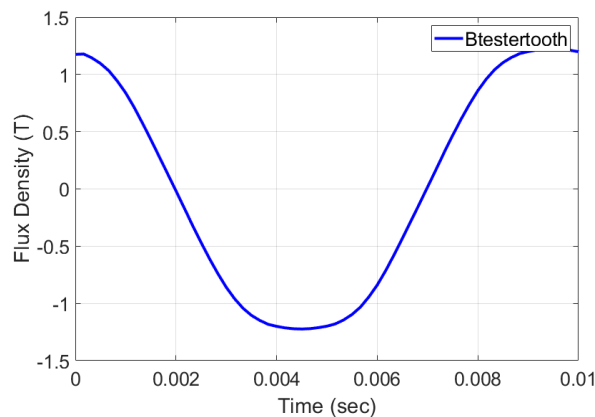


Figure 2.16: The instantaneous values of the tester tooth flux density with 4-pole tester connection in FE simulation

2.6 Analytical Core Loss Calculation

The core loss models used in the commercially available FEA software are based on calculating machine core losses using curve fitting techniques that utilize core loss data provided by steel manufacturers under sinusoidal excitation. But, most of the machines have non-sinusoidal back emf waveforms. The analytical core loss calculations were performed using the mathematical model developed by two colleagues in the research group: Dr. Amirmasoud Takbash and Dr. Maged Ibrahim [29]. This model is based on the calculation using an equivalent sinusoidal waveform of non-sinusoidal magnetic flux density.

The analytically calculated core loss using the magnetic data from the FE simulation and the core loss obtained from the FE simulation are presented in Table 2.1. The comparison of the calculated core loss with the FE simulation results is also provided in the table.

The equivalent frequency and flux density equations for the analytical model are as given by Equation 2.1 and Equation 2.2. The core loss calculation algorithm using the equivalent flux density B_{eq} and equivalent frequency f_{eq} is shown in Figure 2.17. The input data required for the calculation is flux density and volume for the mesh from FE simulation.

$$f_{eq} = \frac{2}{\pi^2} \sum_{k=2}^K \left(\frac{B_k - B_{k-1}}{B_{max} - B_{min}} \right)^2 (t_k - t_{k-1}) \quad (2.1)$$

$$\hat{B}_{eq} = \left(\frac{B_{max} - B_{min}}{2} \right) \quad (2.2)$$

In the equations 2.1 and 2.2, B_k is k^{th} sample of flux density in each mesh element; B_{max} and B_{min} are the maximum and minimum value of a flux density waveform, and $(t_k - t_{k-1})$ is the sampling period. \hat{B}_{eq} is equivalent flux density; f_{eq} is equivalent frequency and K is the total number of samples.

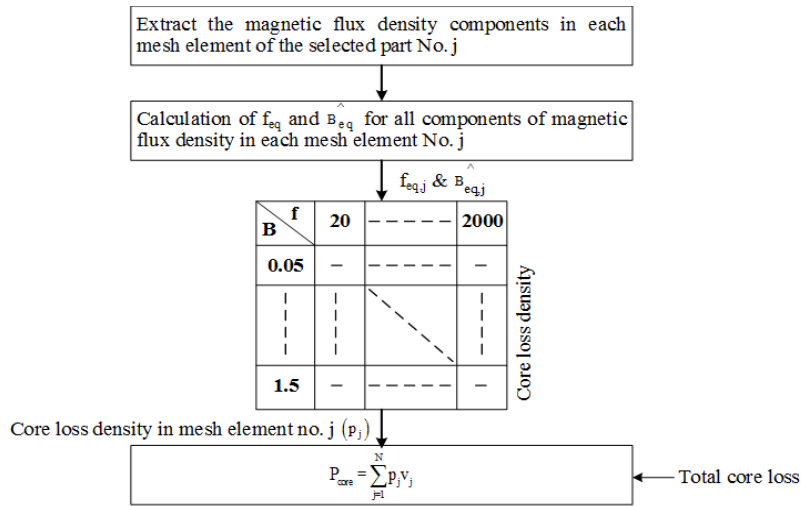


Figure 2.17: Core loss calculation algorithm used for core loss estimation for the new tester and stator [29]

The core loss comparison in Table 2.1 shows a very close match between the simulated and calculated core losses. The simulated and calculated losses are at an excitation of 15 A peak current waveform with 2-pole, 4-pole and 6-pole connection and 60 Hz, 100 Hz 200 Hz and 400 Hz.

Table 2.1: Comparison of simulated and calculated core loss

| Total Core Loss | | | | |
|------------------------|-----------------------|--------------------------------------|-----------------------------------|------------------------------|
| Connection | Frequency (Hz) | FE Simulation¹ (W) | Analytical² (W) | Percentage Difference |
| 2 – Pole | 60 | 60.97 | 62.58 | 2.64 |
| | 100 | 120.39 | 128.93 | 7.09 |
| | 200 | 327.44 | 345.32 | 5.46 |
| | 400 | 940.54 | 960.59 | 2.13 |
| 4 - Pole | 60 | 26.76 | 31.61 | 18.12 |
| | 100 | 51.19 | 61.46 | 20.06 |
| | 200 | 134.67 | 136.99 | 1.72 |
| | 400 | 396.68 | 403.25 | 1.66 |
| 6 - Pole | 60 | 10.73 | 10.66 | - 0.65 |
| | 100 | 20.31 | 20.41 | 0.49 |
| | 200 | 51.82 | 51.92 | 0.19 |
| | 400 | 144.14 | 141.98 | -1.49 |

¹Total core loss consisting of the tester and the stator core loss from FE simulation.

²Total core loss consisting of the tester and the stator core loss calculated using analytical model.

2.7 Summary

In this chapter, a novel core loss tester for the estimation of core loss in an assembled stator stack is presented. The design principle is explained with the need of the new tester design. The dimensions of the tester are determined based on the air gap, the dimensions of the stator under test and the slot loading of the tester. The 3D geometry of the tester and the stator was prepared using SOLIDWORKS. The use of the new core loss tester for core loss estimation with various waveform shapes and different type of electrical machines is presented. The core loss estimation is performed using 2D and 3D FEA simulations. The effect of the number of poles of the tester excitation winding on the flux density distribution in the tester is analyzed by simulating the tester with 2-pole, 4-pole and 6-pole connections. The effect of the excitation frequency was studied by exciting the tester with various frequencies like 60 Hz, 100 Hz, 200 Hz and 400 Hz. Analytical core loss calculation based on the magnetic and dimensional data

obtained from the FE simulation was performed and compared with the simulated core loss data. The simulated and calculated core losses show a matching within 5-7 %.

3. Theory, Development and Construction of New Core Loss Tester

3.1 New Core Loss Tester Structure

The tester is developed to impose a time-dependent magnetic flux of controlled amplitude and frequency in the stator teeth and back iron of the stator under test. The core loss tester is an electromagnetic device made up of a laminated electrical steel core and consists of coils for exciting the tester and stator and coils for measuring the excitation coils for the tester and stator excitation and sensor coils for measuring the magnetic flux density (B) and magnetic field strength (H).

3.1.1 Tester Core

The tester core is shown in Figure 3.1 (a) & (b). The tester core is made up of 351 thin laminations of non-oriented M19 Gauge 29 silicon steel. The outer diameter of the tester is 108.60 mm and inner diameter is 50 mm. The stack length of the tester core is 125 mm. Figure 2.7 shows the 2-D CAD diagram of the tester with dimensions and the 3-D CAD diagram is shown in Figure 3.1 (a). There are 24 laser cut slots in each lamination to accommodate the windings. The slot dimensions and shape are as shown in Figure 2.7 and Figure 3.1 (a) & (b).

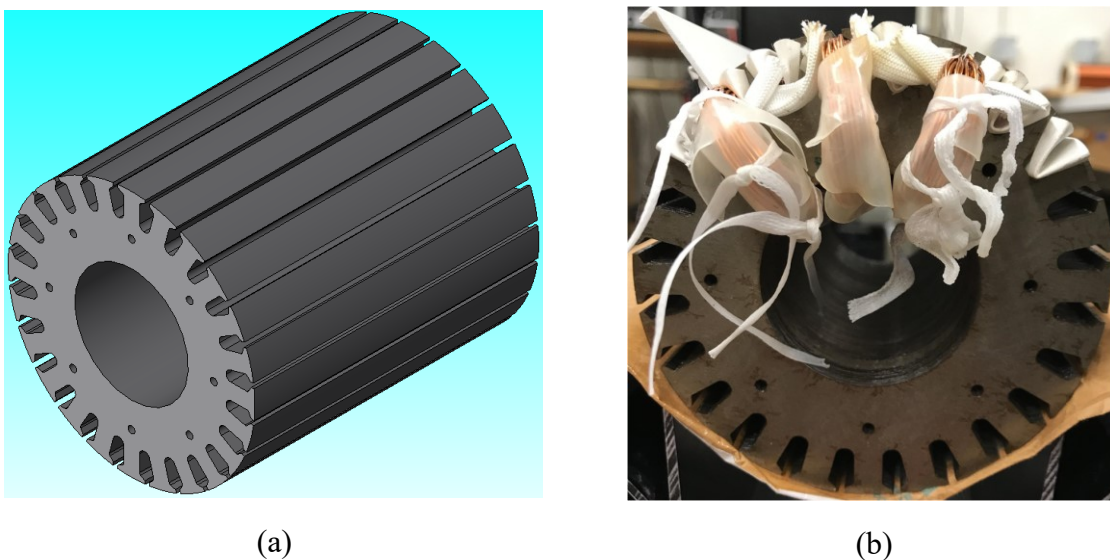


Figure 3.1: The Tester Core (a) 3-D design of the tester core (b) The tester core made up of non-oriented silicon steel during winding process

The edges of slot openings are rounded in order to remove any sharp corners in the magnetic circuit. There are eight holes provided on the laminations to align laminations at the time of stack assembly. The laminations are stacked and pressed together to make the tester stack

shown in Figure 3.1 (b). The individual laminations in the stack are coated with oxide coating on the surface to insulate the laminations from each other.

3.1.2 Excitation Coils

The first winding in the tester is the excitation winding. The excitation winding in the tester serves the purpose of imposing the required current and hence a Magneto Motive Force (MMF) to the magnetic circuit. The excitation coil is wound using Litz wire - a braided bundle of individually enameled copper strands to minimize the skin effect and maximize the current density. The number of strands in Litz wire and thickness of the strands are chosen to maximize the current density and minimize the required area of the slot and the manufacturing cost. The excitation winding is effectively like a toroidal winding as discussed in chapter 2. There are 24 excitation coils in total in the tester, one in each slot. The CAD diagram of the excitation coils is given in Figure 3.2 and the excitation coils during winding process are shown in Figure 3.3.

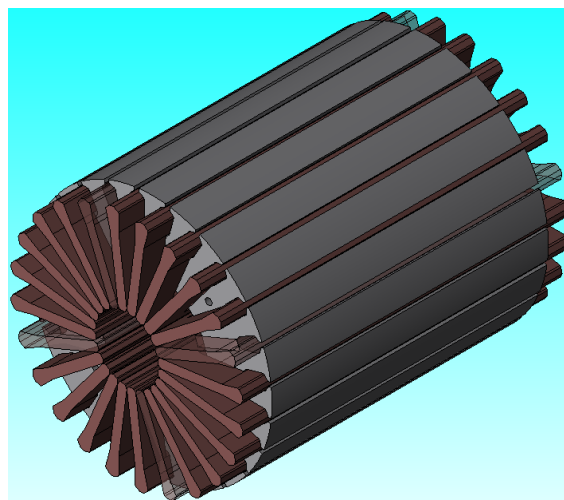


Figure 3.2: The excitation coils in 3-D CAD model



Figure 3.3: The excitation coil during winding process

Table 3.1: Excitation coil winding specifications

| | No. of turns per slot | Wire size (AWG) | No. of strands in conductor per turn |
|-----------------|-----------------------|-----------------|--------------------------------------|
| Excitation coil | 10 | 21 | 6 |

The winding details for the excitation coils are given in Table 3.1. All the excitation coils are left open at one end in order to provide flexibility in the connection as described in chapter 2.

3.1.3 Sensor Coils

There are two popular methods to measure the flux density in the sample under test: needle or tip method and B-coil method. In the needle or tip method, the flux density is calculated by measuring the potential difference between two points on the surface of a steel sheet to which the tips are applied. The needle or tip method is not suitable in this work since the flux density in the tester back iron and teeth have to be measured. In addition, the surface insulation has to be removed to use needle or tip method [30]. The B-coil method is used more frequently and is more reliable.

The average flux density in any material can be detected by means of a B-coil (also known as “search coil” or “pick-up coil”). The sensor works on the principle of Faraday’s law of electromagnetic induction. The induced voltage is proportional to the rate of change of flux density, the number of turns of the coil, and the area enclosed by the coil as shown in Figure 3.4 and Equation 3.1.

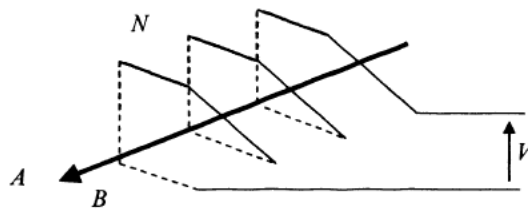


Figure 3.4: The concept of a search coil or pick-up coil technique: V - voltage induced in the coil, N - number of turns in the coil, A - area enclosed by the coil, B - flux density

$$V = -N.A.\frac{dB}{dt} \quad (3.1)$$

Where: N – number of turns of coil (dimensionless), A – cross-section area of the coil [m^2], dB/dt – rate of change of flux density with respect to time [T/s].

Therefore, the flux density waveform can be obtained by integrating the induced voltage in the coil:

$$B = -\frac{1}{N \cdot A} \cdot \int V dt \quad (3.2)$$

The B-coil, presented in Figure 3.4, detects the flux density averaged over the area A .

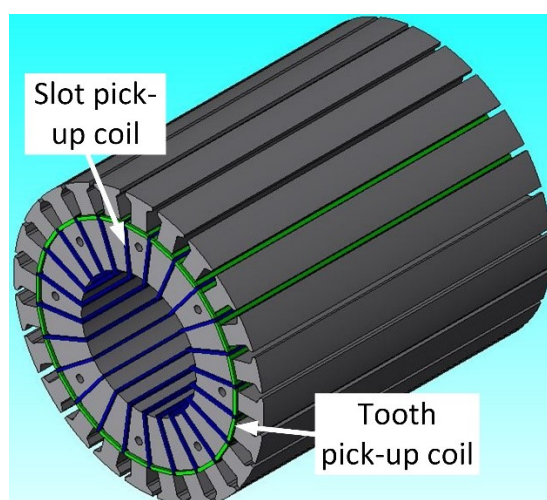


Figure 3.5: Slot pick-up coil and Tooth pick-up coil in 3-D CAD diagram

There are two types of pick-up coils used in the analyzed tester, namely, slot pick-up coils and tooth pick-up coils as shown in Figure 3.5. There are in total 24 slot pick-up coils, one for each slot. The slot pick-up coils are useful to sense the flux density in the tester back iron. There are also 24 tooth pick-up coils, one around each tooth as shown in Figure 3.5. The tooth pick-up coils sense flux density in the tester tooth to measure the rotational flux region at the tooth root in the tester. The winding specifications for the slot and tooth pick-up coils are provided in Table 3.2.

Table 3.2: Slot and tooth pick-up coil winding specifications

| | No. of turns per slot | Wire size (AWG) | No. of strands in conductor per turn |
|--------------------|-----------------------|-----------------|--------------------------------------|
| Slot pick-up coil | 3 | 24 | 1 |
| Tooth pick-up coil | 3 | 24 | 1 |

3.2 Development of the Tester

The tester core as shown in the Figure 3.1 (a) & (b) was designed in the PEER group research laboratory by Dr. Maged Ibrahim as discussed in chapter 2. The tester core was assembled with the help of a machine manufacturer by stack pressing and gluing using the laser cut laminations covered with oxide coating for inter laminar insulation. With a fill factor of 49.4 %, it was not possible to perform the winding using a machine and hence had to be hand wound. The copper conductors of the sizes discussed in Table 3.1 and Table 3.2 in the above sections are used for winding.

During the process of winding the tester core, the first step was to insulate the windings from the tester core. The windings are electrically insulated from the tester core using NOMEX[®] 410-insulation paper of 10 mil (0.25 mm) thickness as shown in Figure 3.6 (a). In the inner portion of the tester core, the winding coils are insulated using heat shrinkable insulating tube as shown in Figure 3.6 (b).

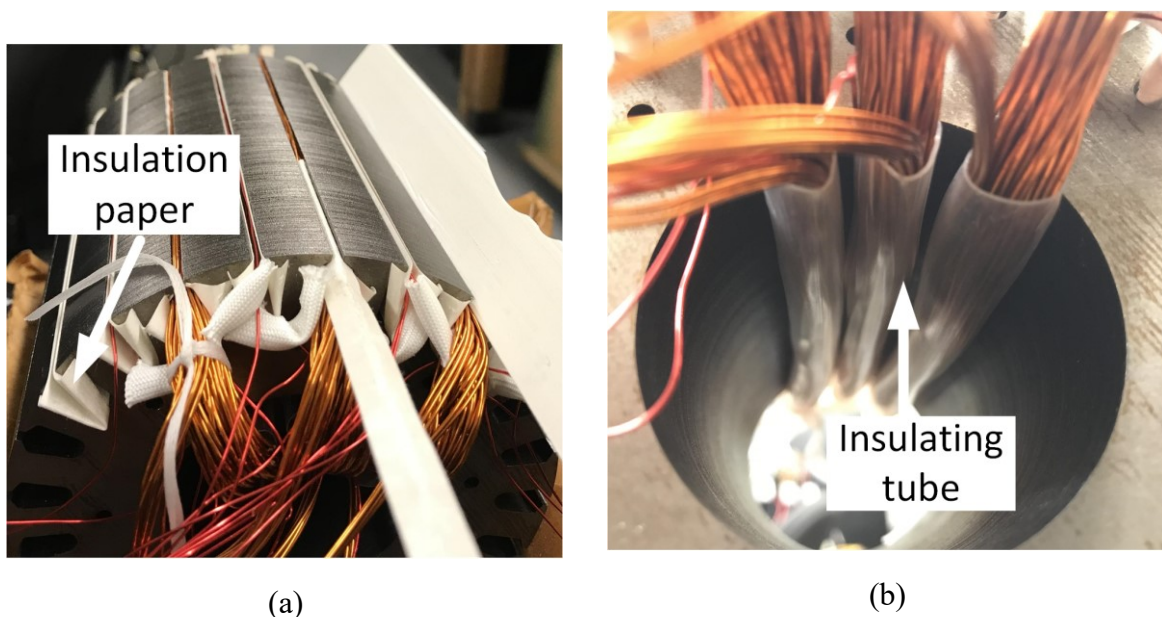


Figure 3.6: (a) Insulation paper to insulate winding from the tester in slot (b) Insulating tube to insulate the winding in the inner portion on the tester

After inserting the insulation papers into the tester core slots, the sensor coils were inserted first during the winding process. The slot pick-up coils and the tooth pick-up coils are inner coils in the winding as shown in the Figure 3.7 and Figure 3.8. The excitation coils are wound over the sensor coils in the tester core slots as indicated by Figure 3.7 and Figure 3.8. The end windings of the tooth pick-up coils are insulated from the tester core using braided insulating sleeves as shown in Figure 3.8.

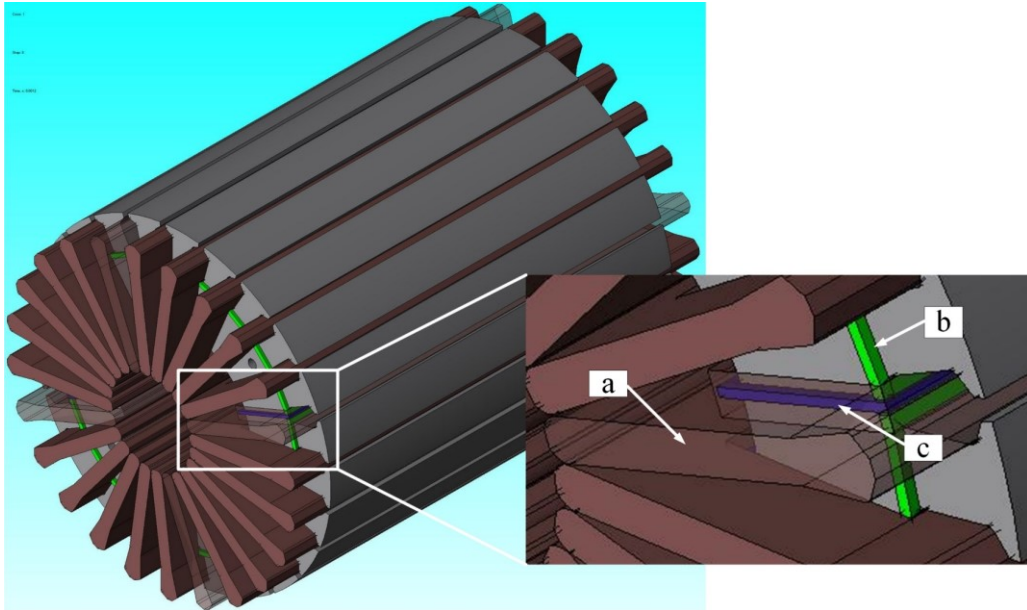


Figure 3.7: CAD diagram of the tester winding (a) Excitation coil (b) Tooth pick-up coil (c) Slot pick-up coil

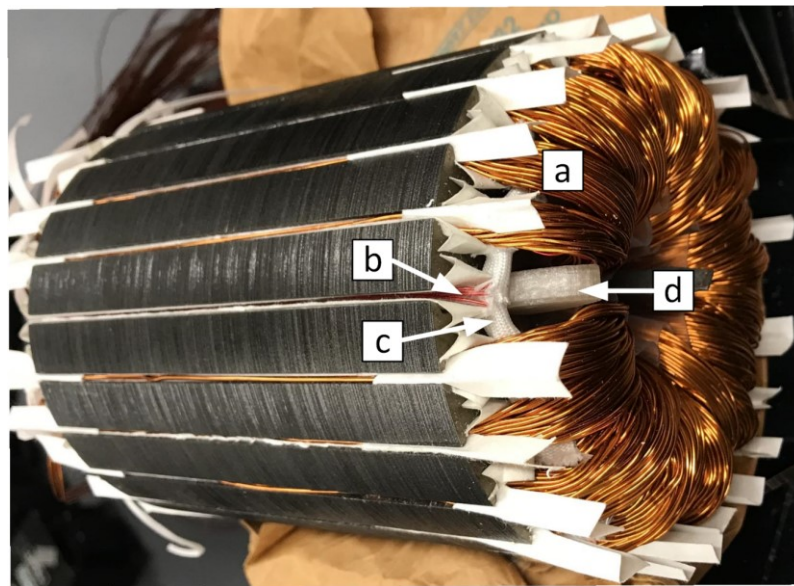


Figure 3.8: The tester core and winding coils (a) Excitation coil (b) Sensor coil (c) Insulating sleeve (d) End-winding spacer

The excitation coil windings are toroidal coils and the end windings will have no effect on the flux distribution in toroidal windings. But, the unequal length of the coils will result in unequal resistance, which ultimately affects the voltage drop in the coils. Therefore, the shape and length of the end winding is kept equal in all the coils. This was done using a small plastic part designed and 3-D printed as shown in Figure 3.8 (d). This plastic piece was inserted during the winding process and removed later after the winding process was finished to maintain the same shape and equal end winding overhang in all the coils. In order, to properly accommodate all the coils in the inner portion of the tester and to keep the total length of the coil equal, the



Figure 3.9: Tester windings during the winding process

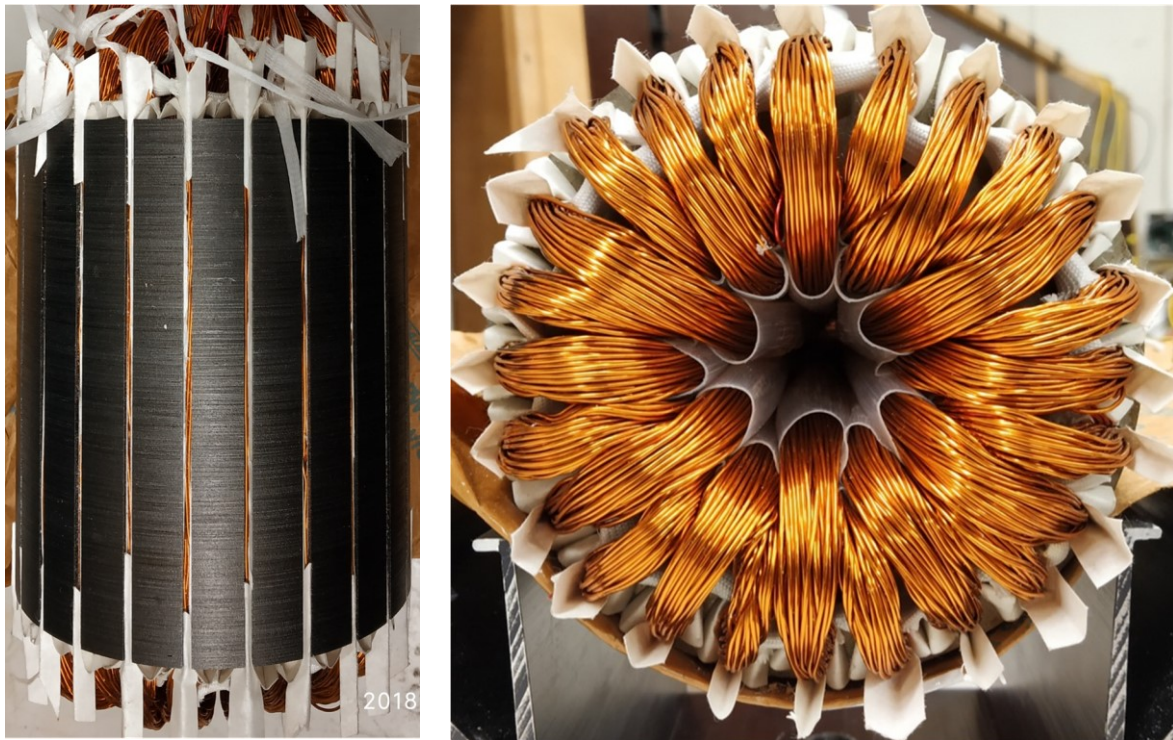


Figure 3.10: The tester with completed winding

excitation coils were wound alternatively as shown in Figure 3.9. The alternate slot coils were wound first and then the remaining coils were wound in order to get uniformly wound coils in all the slots. The completed winding of the tester is shown in Figure 3.10.

As discussed earlier, the fill factor of the tester winding is 49.4%, which is quite high. The excitation winding can reach a current density of 21 A/mm^2 with this high value of fill factor. This high value of fill factor makes it difficult to insert wedges in the wound slot over the winding to secure and protect winding in the slots. Therefore, in order to secure the

windings in the slots, the top portion of the slots is filled with glue as shown in the Figure 3.11 (a). The glue filled in the slots will also act as an insulation between the excitation coil and the top edge of the tester slot. The end-connections of the excitation coil are insulated from each other by using insulation paper as shown in Figure 3.11 (b).



Figure 3.11: The tester with (a) Glue filled slots to insulate excitation coils from the top edge of the slots (b) Excitation coil end-connections separated from each other with insulation paper

3.3 Tester Setup

The tester winding is completed as discussed in the previous section. This section discusses the assembly of the supporting structure of the tester and the terminal connections. As discussed in the previous section and chapter 2, both ends of the coils are kept open in order to allow flexibility in terms of the connection and the number of poles. The tester is mounted vertically and supported at the bottom as shown in Figure 3.12 by a specially designed support structure. The space around the tester on the tester setup will provide the base support for stator to be tested. The stator under test will rest on the wooden support cut with precise length in order to align the tester and the stator. The connection terminals from all three types of coils are brought to the terminal strips attached on both sides of the tester on the wooden board that supports tester. These connections from the terminal strips are connected to the terminal box. The terminal box houses the fuse and the connection plugs to connect the excitation coils and the sensor coils with other equipment in the experimental setup. A fan is mounted below the tester base as shown in Figure 3.13 in order to make sure that enough air circulation is available to remove heat from the tester windings and core. Acrylic sheets cover terminal plates to protect the operator from electrical hazard.

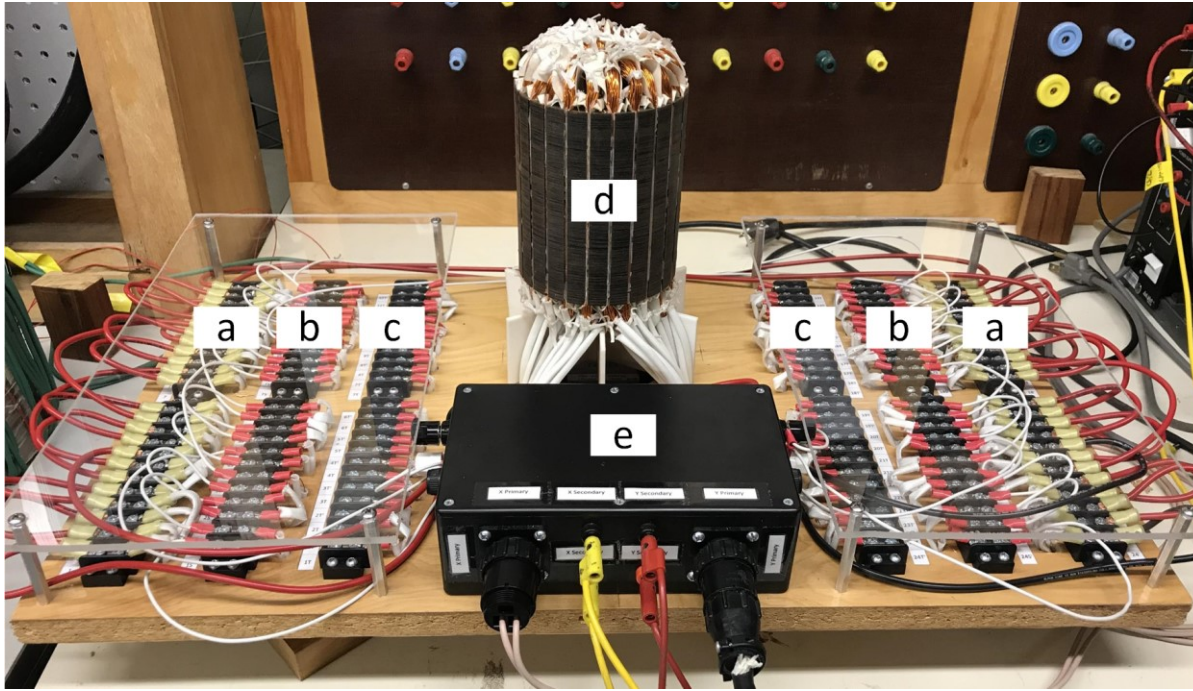


Figure 3.12: Tester setup (a) Excitation coil terminals (b) Slot pick-up coil terminals (c) Tooth pick-up coil terminals (d) Tester (e) Terminal box

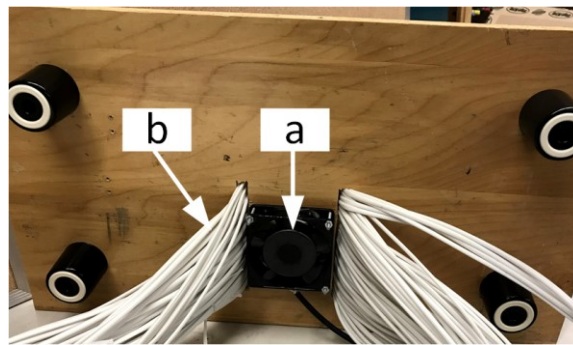


Figure 3.13: The tester setup (a) Cooling fan (b) Winding coil leads

3.4 Experimental Setup

This section explains the experimental setup to perform the core loss measurement and magnetic characterization of the stator stack. The setup can be used to perform the basic measurements, which include pulsating core losses and rotational core losses under the influence of rotating magnetic field in the electrical stator exerted by radial flux rotating electrical machines.

A block diagram of the experiment setup is given in Figure 3.14. MATLAB Simulink[®] software is used to generate two arbitrary excitation waveforms phase shifted by 90° degree. A dSPACE (DS1103) real time simulation controller board is used for the real time simulation and the DAC and ADC operation of the excitation signal and sensor coil signals respectively.

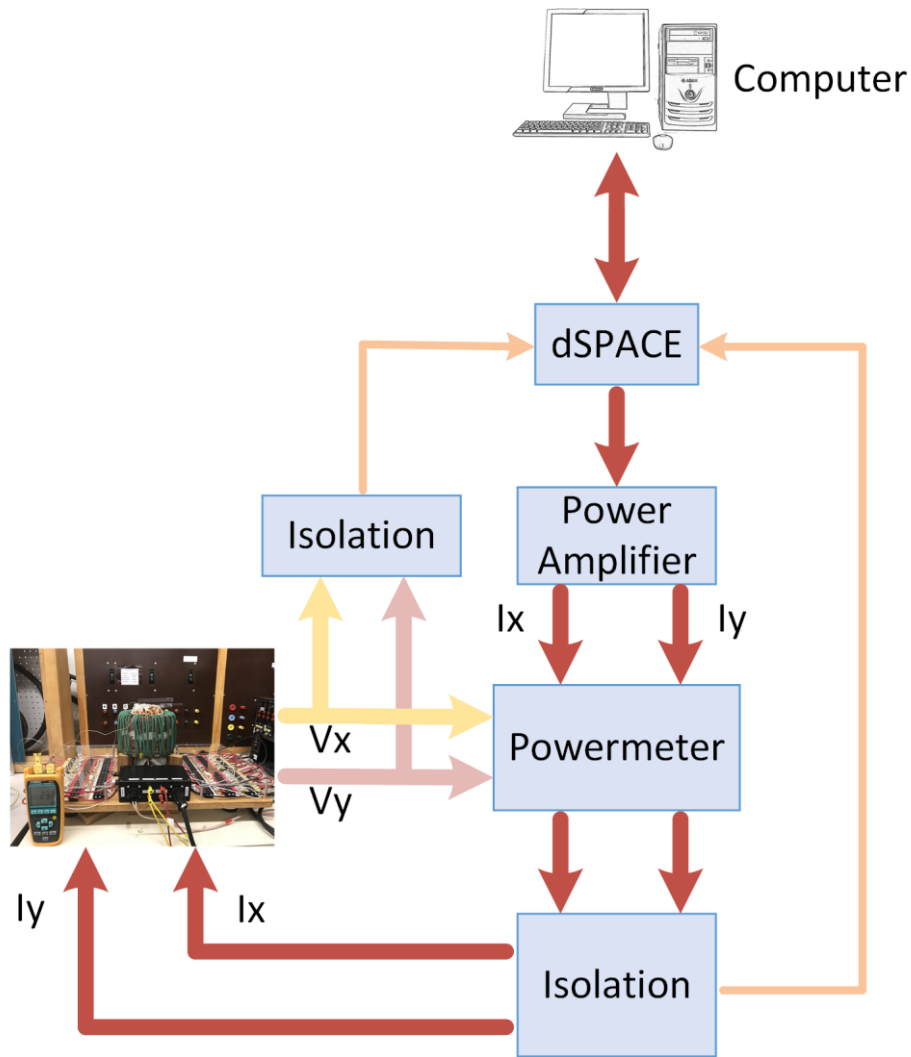


Figure 3.14: The experimental setup block diagram

A photograph of the experimental setup for the core loss measurement using the new tester is shown in Figure 3.15.

The AETECHRON[®] 7224 accurate, high power, high bandwidth, low noise and low distortion linear amplifiers are used to amplify the excitation signals. Two YOKOGAWA[®] 2533 digital power meters are used to measure the core losses in the setup, one for each phase. High gain and low distortion voltage isolation box is used to measure induced emf in the sensor coils. The excitation current in the excitation coils is measured by using YOKOGAWA 701933 current probes. The thermometers and thermocouples indicate the temperature of the core and the winding.



Figure 3.15: The experimental setup (1) Computer (2) dSPACE® DS1103 controller (3) Power amplifier (4) Power meters (5) Voltage/current isolation (6) Tester setup with stator under test (7) Thermometer and thermocouples

3.5 Working of the New Tester

The experimental setup employs the new tester to carry out core loss measurements in the stator cores of electrical machines. MATLAB Simulink® software generates the excitation waveforms with the desired magnitude, frequency and wave shape. This allows flexibility to the user in choosing any physically realizable excitation waveform, especially the non-sinusoidal waveforms usually found in the electrical machines driven by power electronics converters.

The waveforms generated are converted to voltage signals by the DACs inside dSPACE (DS1103). The two linear power amplifiers amplify these signals. The linear amplifiers operate in the current control mode in order to feed the excitation current signal to the tester. The two signals are phase shifted by 90° , which results in a two-phase excitation. The current signals are fed to the stator core loss tester through the power meters and current isolator in order to measure the excitation current. Current signal I_x excites the phase x coils and I_y excites the phase y coils.

The total core loss including the tester loss and the stator core loss is measured by feeding the excitation current and the induced emf in the tester to the power meter as defined by ASTM A348 [7]. There are four output signals that can be obtained from the test setup: I_x , I_y , V_x and V_y , which are related to the excitation current in phase-x, excitation current in phase-y, induced emf in phase-x sensor coils and induced emf in phase-y sensor coils. In addition to these signals, all the tester teeth have a tooth sensor coil, which gives the induced emf in the tester tooth. These signals are sent to dSPACE (DS1103) for ADC conversion, which is linked to MATLAB Simulink[®], thus allowing digital monitoring and control of all the generated and sensed signals. The MATLAB Simulink[®], schematic for generating and sensing of the required waveforms is as shown in Appendix.

3.6 Testing, Calibration and Loss Separation Procedure

The watt-metric method is used in this work, which is easy to implement for core loss measurement and it gives direct reading of core loss using a wattmeter. The stator core under test should be inserted over the core loss tester shown in Figure 3.12. The air-gap should be properly adjusted and the stator stack should be perfectly aligned vertically with the tester in order to excite the stator under test uniformly in all the directions with the rotating magnetic field. When the tester is excited, it generates a rotating magnetic field that is similar to the air gap field in AC machines.

The reference quantity used in the testing is the peak magnetic flux density (B_p). The peak flux density in the tester back iron is calculated by integrating the induced emf waveforms in the slot pick-up coils in real time. The tester back iron to stator back iron flux density ratio can be calculated by using pick up coils in the stator under test. This process can be repeated for a few stators of the same material and a ratio can be defined and used in the core loss calculation. This initial ratio calibration process will help in core loss measurement without using the stator pick up coils at the later stage of the testing as the tester to stator flux density ratio is already defined. The calculated core loss can be easily related to the particular flux density of the stator under test.

The wattmeter measures core loss as explained in the previous section. The measured core loss by the test system includes the core loss of the stator core under test as well as the core loss of the tester core. Therefore, a method is developed to separate these two losses. A ring tester as shown in Figure 3.16 is used to measure the specific core loss of the tester material.

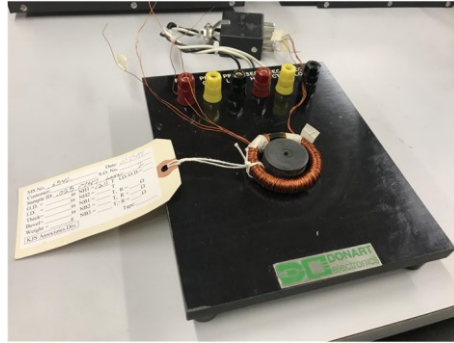


Figure 3.16: Ring tester for the tester calibration

The geometry of the ring tester is similar to the core of the new tester and the radial flux electrical machines, as the flux forms closed path inside the ring. This makes the ring test an ideal method for the new tester calibration. The weight of the tester is a known quantity and by using the specific core loss and the tester weight the total core loss of the tester at the frequency of interest can be calculated.

The next step in loss separation procedure is to calculate the total core loss of the stator stack under test by subtracting the tester core loss from the total measured core loss. The stator specific core loss can be calculated by using the total core loss of the stator and known weight of the stator. Note that the tester core loss obtained using the ring tester is under the pulsating excitation not the rotating excitation.

3.7 Summary

The detailed structure of the new core loss tester was discussed along with the description of various components, the core structure and the winding details. The prototype development procedure for the new core loss tester was elaborated with the techniques used for the winding and the new approach used for the winding with high fill factor. The experimental setup to perform core loss measurement using the new tester and the different equipment used in the setup were discussed with appropriate images. Finally, the testing procedure and the loss separation method was discussed to perform the core loss measurement using the new core loss tester.

4. Experimental Results and Comparison with FEA Simulation Results

The core loss measurements are carried out using the new prototyped core loss tester. The core losses are measured for different cases by using the watt-metric method according to the ASTM A348/A348M standard [7]. The measured losses are separated according to the procedure explained in previous chapter. In this chapter, the measurement results from the new core loss tester and an Epstein frame are compared. Discrepancies in the core loss measured by the new tester and the core loss measured by Epstein frame are provided and analyzed.

The core loss measurements were carried out by applying a rotating magnetic field to realize the radial flux distribution in the actual electrical machines.

4.1 Tester Calibration using Ring Tester

A ring test was performed using a custom designed commercially available test bench in which a sinusoidal excitation is used according to the ASTM A927/A927M standard [8]. A ring sample was made using the tester core material (M19G29) with 17 rings in the core was used for the ring test. The ring tester used for the core loss measurement has 120 primary turns and 120 secondary turns. The specific core loss measured at different frequencies of interest using the ring tester are shown in Figure 4.1. The tester calibration is performed using a pulsating excitation, since the calibration under rotational excitation was not possible due to the limitation discussed below.

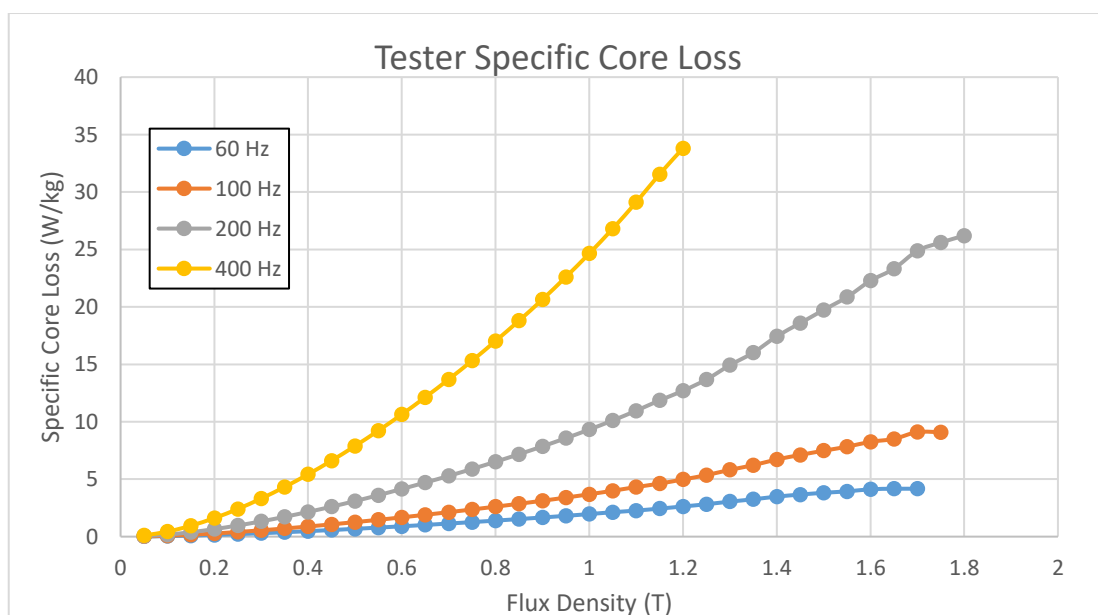


Figure 4.1: Specific core loss of the tester measured using the ring test according to the ASTM A927 standard

A more accurate calibration is obtained if the tester and the stator under test are made of the same material. This is because there is no need of loss separation between the materials used in the tester and the stator. The specific core loss can be simply calculated by dividing the total measured loss by the total weight of the tester and the stator under test. Due to unavailability of the stator made up of the same material as tester, this technique for tester calibration was not used in this research work.

4.2 Tester to Stator Flux Density Ratio Calibration

As discussed in chapter 2, the primary purpose of the new tester is to measure the core loss in assembled stator stacks of electrical machines before the final machine assembly. To relate the core loss with the particular stator flux density using the measurement procedure explained in chapter 3, the tester to stator back iron flux density ratio must be defined accurately. This will enable the core loss estimation without using the stator sensor coils and there will be no need to wind any excitation or sensor coils on the stator under test. This will allow the stator testing to be done directly on the assembly line.

To define the tester to stator flux density ratio, the peak back iron flux density for both the tester and the stator are recorded for different excitation levels and different frequencies. The same test can be performed using different stators made up of the same material. The results from all these tests will give the ratio of the tester to stator back iron flux density. This ratio will serve as a calibration for the particular tester with which all the tests are performed. Once the ratio is calibrated, there is no need to wind sensor coils on the stator under test to estimate the flux density in its back iron. The calibration ratio will relate the tester flux density to the stator with an acceptable accuracy. The accuracy of the ratio calibration process depends on the amount of testing data collected during the calibration and calibration conditions (i.e. ambient, tester and stator temperature, the accuracy of flux density estimation method, number of repeated tests performed etc.).

The above ratio calibration process was employed in this research work. There was only one stator available to test the proposed method, so multiple tests were performed on the same stator and the results were repeatable. The ratio calibrated for the 2-pole connection for 60 Hz, 100 Hz, 200 Hz and 400 Hz is shown in Figure 4.2. The ratio calibration graph for the 4-pole connection and excitation frequencies of 60, 100, 200 and 400 Hz is shown in Figure 4.3 and Figure 4.4 shows the same graph for the 6-pole connection.

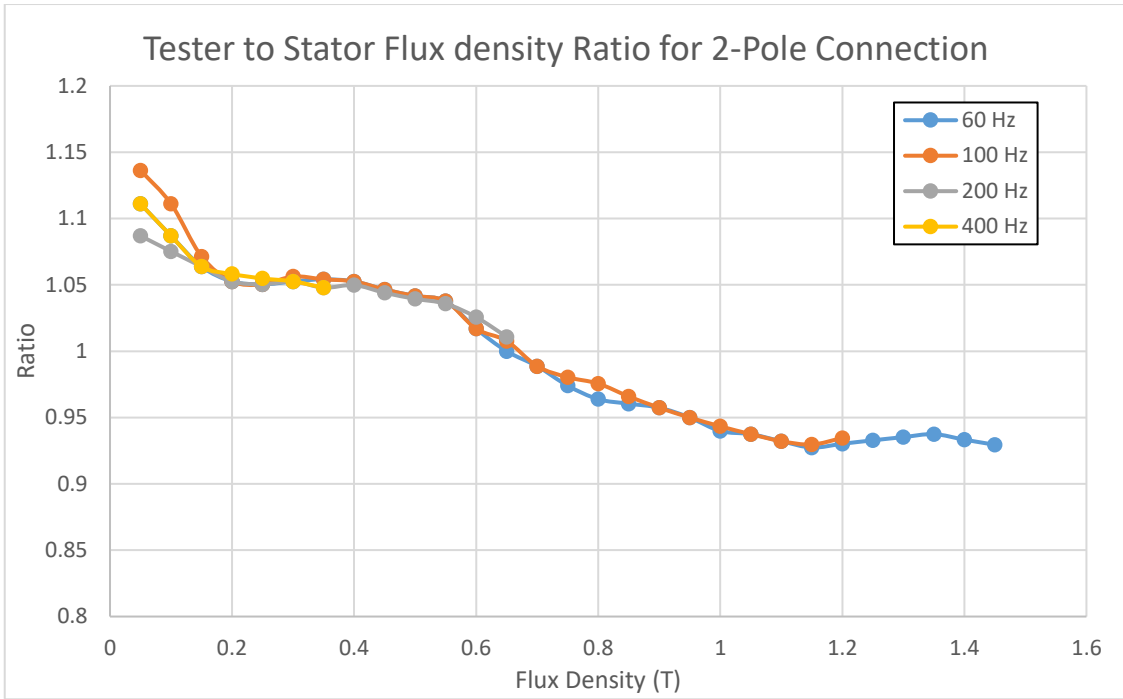


Figure 4.2: Tester to stator back iron flux density ratio for 2-pole connection at various frequencies

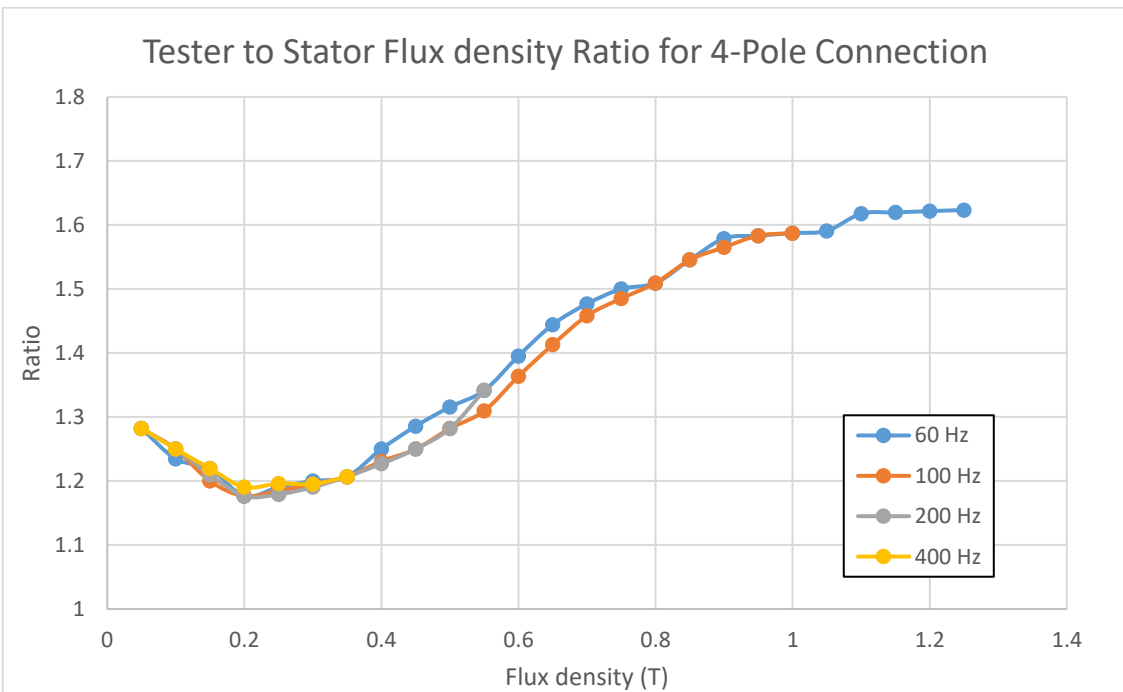


Figure 4.3: Tester to stator back iron flux density ratio for 4-pole connection at various frequencies

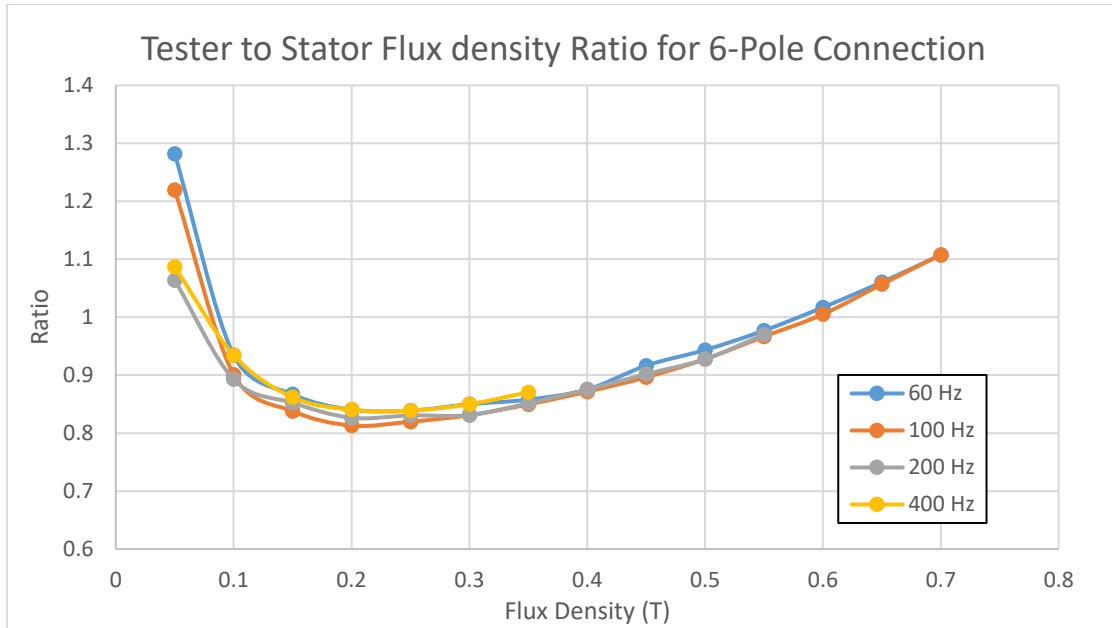


Figure 4.4: Tester to stator back iron flux density ratio for 6-pole connection at various frequencies

4.3 Experimental Results

The measurements were carried out on a 36-slot stator made up of M36 29 gauge silicon steel. The stack length of the stator is 125 mm, inner diameter is 109 mm and outer diameter is 180mm. The weight of the tester is 5.62 kg and of the stator is 11.39 kg. The stator under test and the tester dimensions are shown in the Figure 4.5.

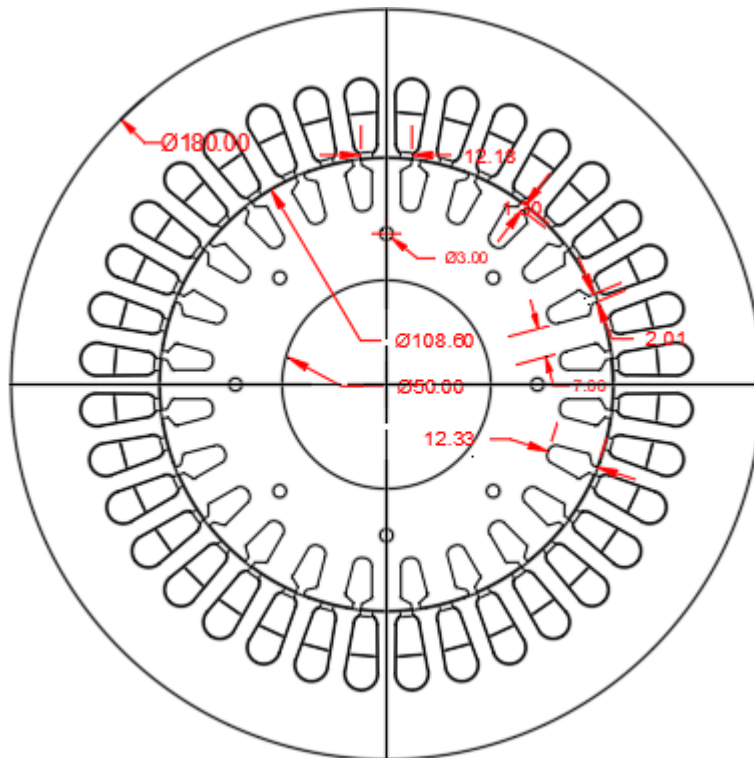


Figure 4.5: The stator and the tester CAD diagram with dimensions in mm

4.3.1 Signals Obtained from the Stator and the Tester Sensor Coils

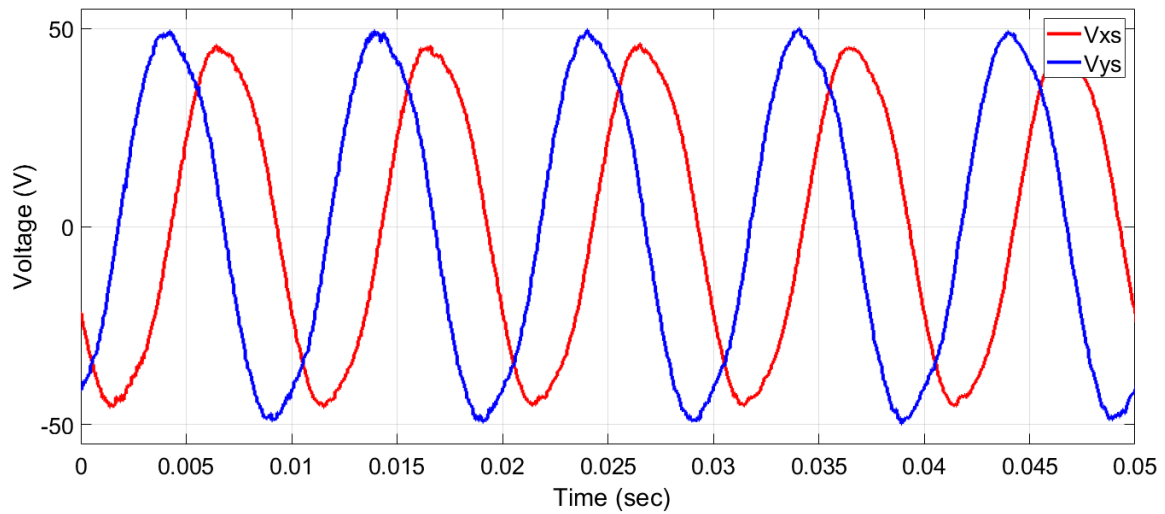


Figure 4.6: The instantaneous output voltage signals at 100 Hz and 4-pole winding connection in the tester sensor coils (slot pick-up coils)

The output voltage signals obtained from the sensor coils in the tester made up of M19 gauge 29 silicon steel with the 4-pole winding connection are presented at a flux density of 1 T and a frequency of 100 Hz. The two tester back iron induced emf signals V_{xs} and V_{ys} (phase shifted by 90°) and sensed by the two sensor coils for accurate measurement are shown in Figure 4.6. These signals experience some distortion, but the integration reduces the distortion when these signals are used to construct the tester back iron flux density signals B_x and B_y as shown in Figure 4.7. The tester back iron flux density is the reference quantity in all the measurements.

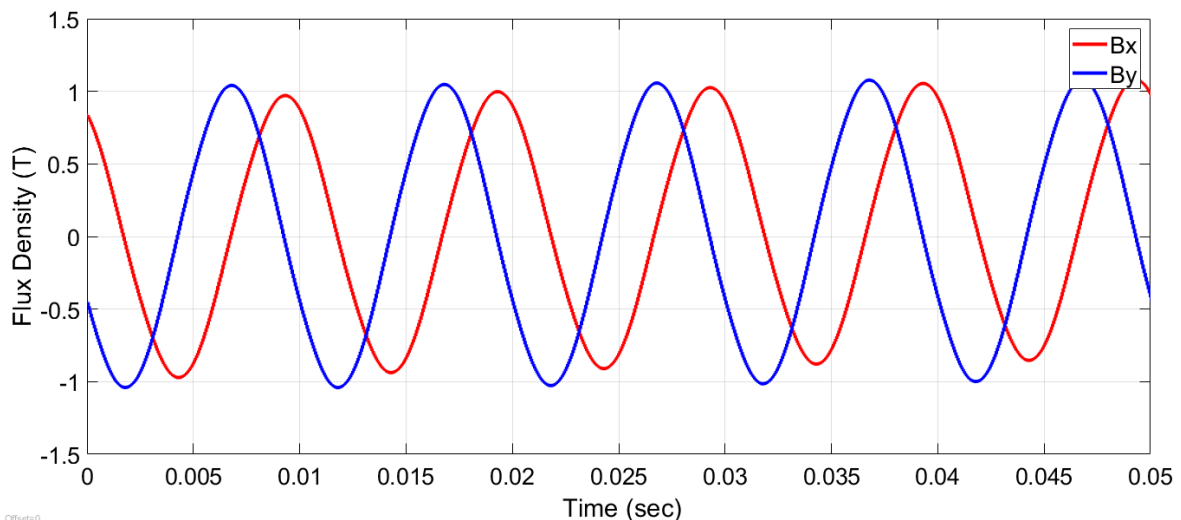


Figure 4.7: The instantaneous values of the magnetic flux density at 100 Hz and 4-pole winding connection in the tester constructed by integrating the instantaneous voltage waveforms of the tester sensor coils (slot pick-up coils)

Figure 4.8 shows the signals obtained from the tooth sensor (pick-up) coils with the 4-pole winding connection, 100 Hz frequency and 1.45 T flux density in the tester tooth. This signal is used to obtain the tooth flux density in the tester. The tooth flux density study is important as the tooth root contains rotational flux region, which results in higher core loss in

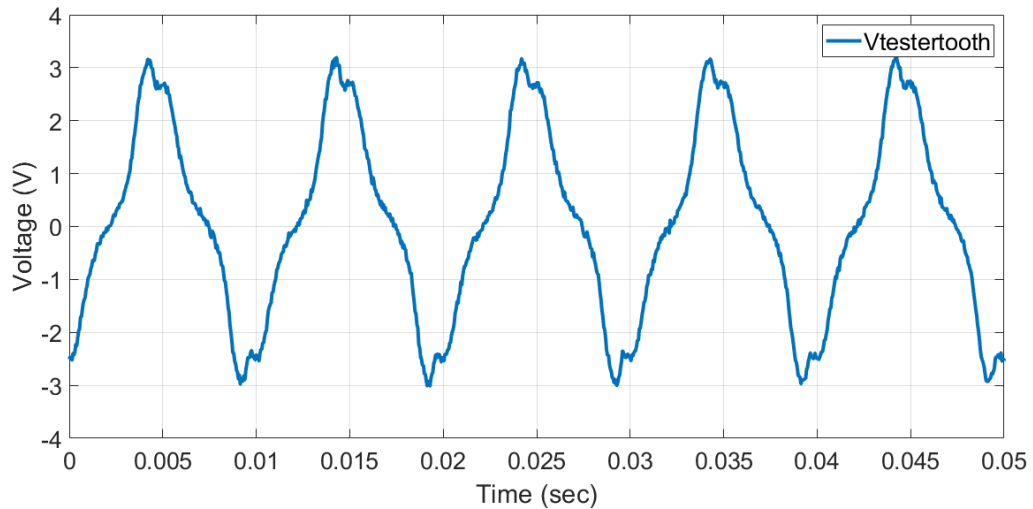


Figure 4.8: The instantaneous output voltage signal at 100 Hz and 4-pole winding connection in the tester tooth sensor coils (tooth pick-up coils)

the tooth root region [31] and forms local hot spot in electrical machine cores with poor ventilation. The distortion in the waveform of Figure 4.8 is due to the higher flux density of 1.45 T in the tester tooth, which is approaching saturation. The signal obtained from the stator sensor coils during the tester to stator flux density ratio calibration process at 100 Hz and 4-

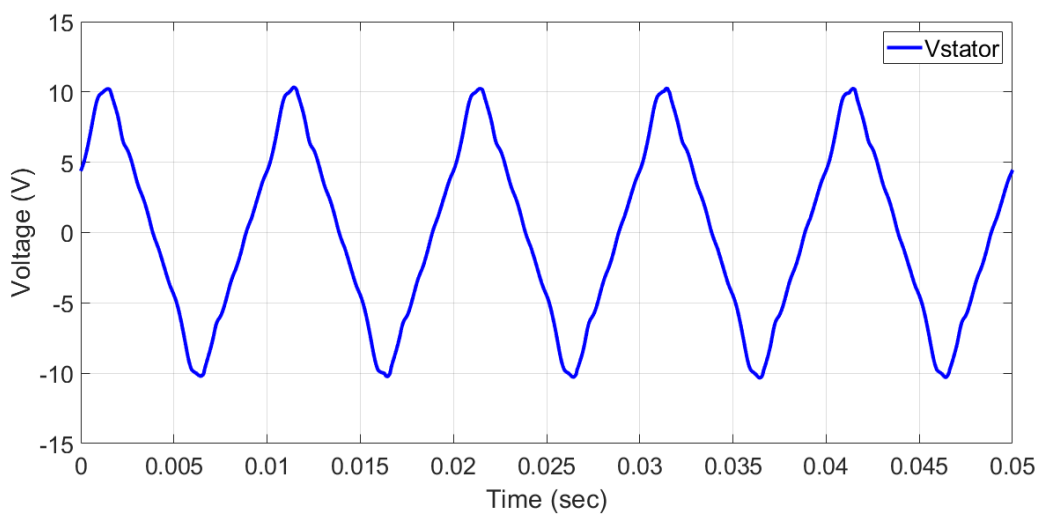


Figure 4.9: The instantaneous output voltage signal at 100 Hz and 4-pole winding connection in the stator back iron sensor coils (stator slot pick-up coils) during the tester to stator flux density ratio calibration

pole connection is shown in Figure 4.9. The flux density waveform is given in Figure 4.10. The validity of the tester results can be confirmed by comparing the waveforms presented in this section by the simulation results presented in section 2.5. All the experimental and simulated waveforms are closely matching with each other.

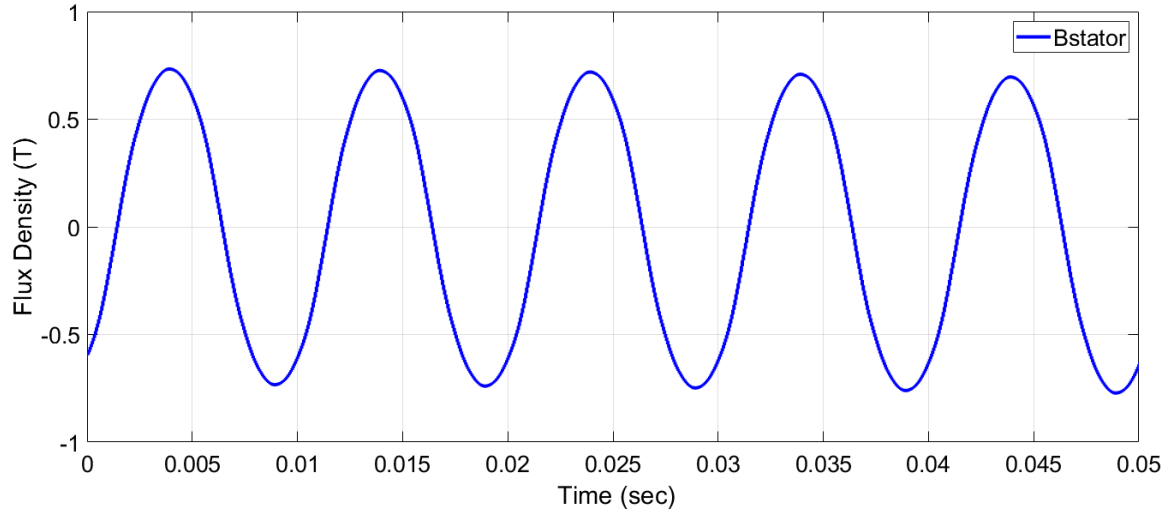


Figure 4.10: The instantaneous values of the magnetic flux density at 100 Hz and 4-pole winding connection in the stator constructed by integrating the instantaneous voltage waveforms of the stator sensor coils (stator slot pick-up coils)

4.3.2 Core Losses Measured Under Influence of Rotational Magnetization

Both the excitation windings of the tester are excited simultaneously with equal magnitude sinusoidal waveforms at four frequencies of interest (60 Hz, 100 Hz, 200 Hz and 400 Hz), with a phase shift of $\Phi = 90^\circ$ between them. The resulting fluxes creates a clockwise rotational magnetic field in the tester and the stator under test. The core losses in the stator are measured at different frequencies as well as at different number of poles (2-pole, 4-pole and 6-pole) in the excitation winding of the tester.

4.3.2.1 Core Loss Measurement at Different Frequencies

Figure 4.11 represents specific core losses in the stator under test made up of laminations with M36 29 gauge silicon steel with 36 slots in the laminations and 125 mm of stack length. The specific core loss curves shown in Figure 4.11 are obtained using a 2-pole winding connection in the excitation winding of the tester at four different frequencies indicated in the plot. These losses are separated from the total losses measured according to the loss separation method explained in section 3.6 and section 4.1.

As already proved by earlier works in the field of core loss measurement, in silicon steel, the specific core loss increases with the increase in the excitation waveform frequency.

Figure 4.11 also agrees to this for the stator excited with 2-pole excitation winding connection using the new tester. Figure 4.12 and Figure 4.13 illustrates the same for 4-pole and 6-pole excitation winding connection respectively.

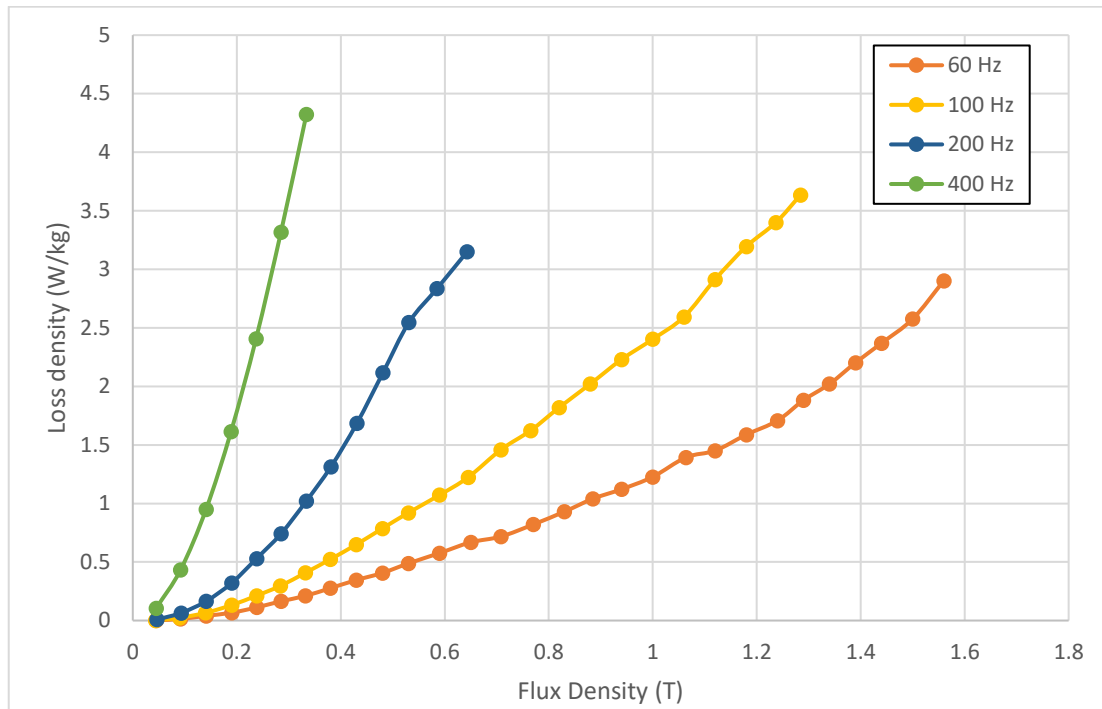


Figure 4.11: Specific core loss of the stator under test measured with the new core loss tester with 2-pole connection of the excitation coil winding

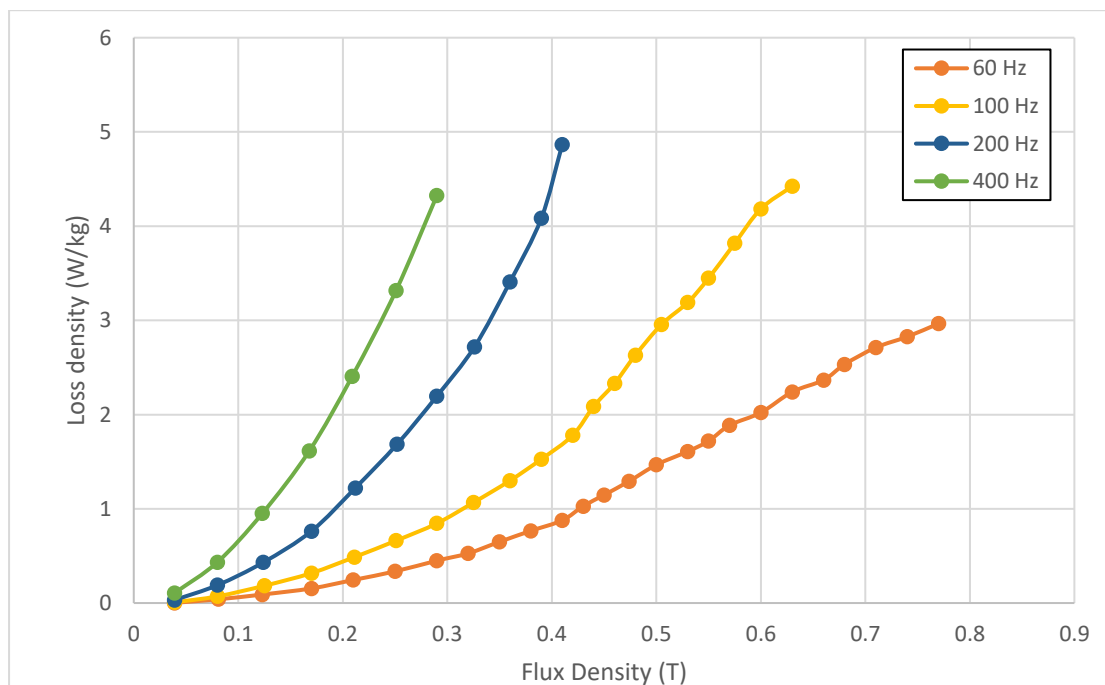


Figure 4.12: Specific core loss of the stator under test measured with the new core loss tester with 4-pole connection of the excitation coil winding

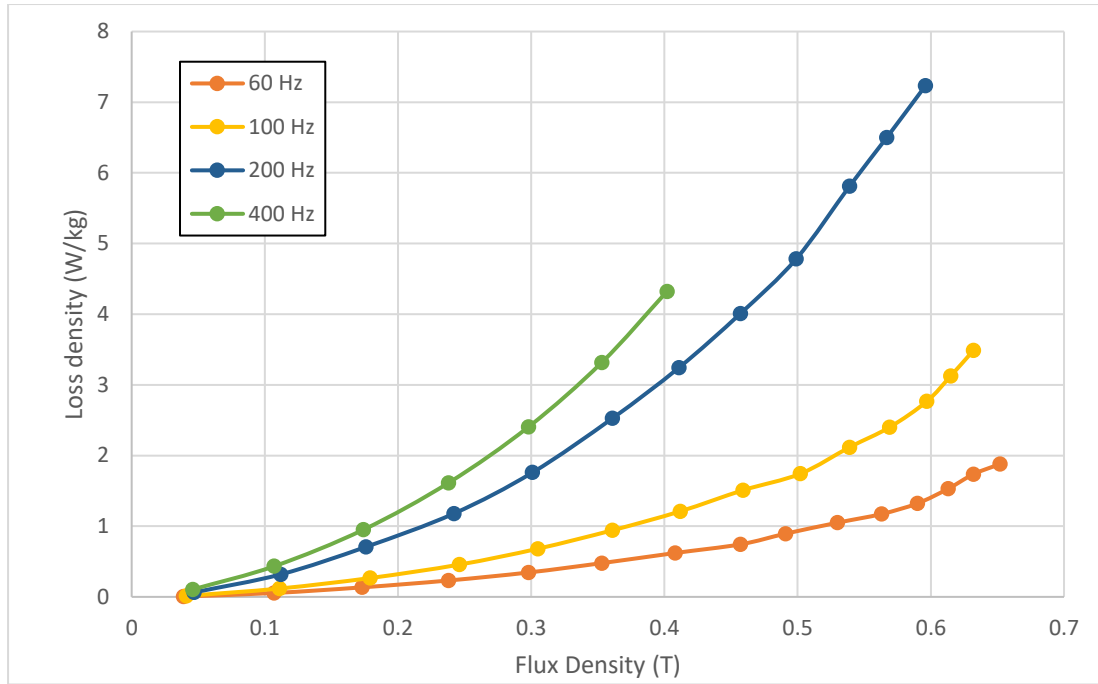


Figure 4.13: Specific core loss of the stator under test measured with the new core loss tester with 6-pole connection of the excitation coil winding

4.3.2.2 Core Loss Measurement with Different Number of Poles

In order to study the effect of change in number of poles on core loss of the stator, the core loss was measured with different number of poles in the excitation windings of the tester. This was achieved by changing the connection of the winding terminals on the terminal plate of the tester setup shown in Figure 3.12. During the measurement process, the temperature of the excitation winding, tester core and the stator core was maintained between 25° C and 32° C by using a cooling fan as explained in section 3.3.

The core loss measured with the 2-pole, 4-pole and 6-pole connections at frequencies of 60 Hz and 100 Hz is shown in Figure 4.14. It is evident from the plot that at both the frequencies the 4-pole connection has the highest specific loss among all the three excitation winding number of pole combination. The 2-pole connection has the least specific core losses.

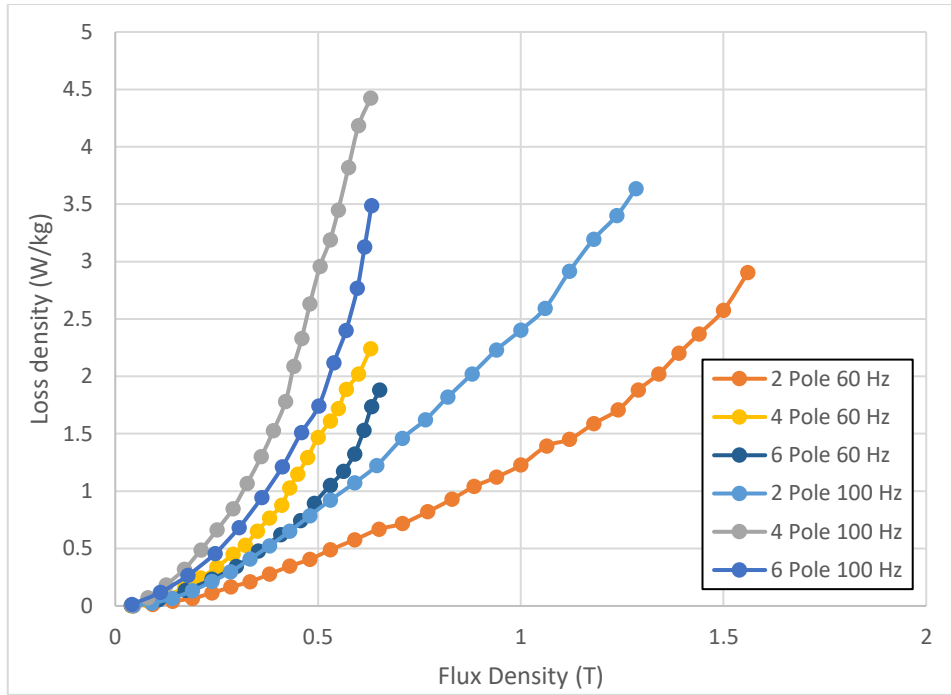


Figure 4.14: Specific core loss of the stator under test measured with the new core loss tester with 2-pole, 4-pole and 6-pole connection of the excitation coil winding at 60 Hz and 100 Hz frequency

The same results are observed at the frequencies of 200 Hz and 400 Hz and are shown in Figure 4.15. This approach of core loss estimation with different numbers of poles combination will be helpful in choosing the type of steel, which will give best performance with the lowest losses at the desired number of poles in the electrical machine design procedure.

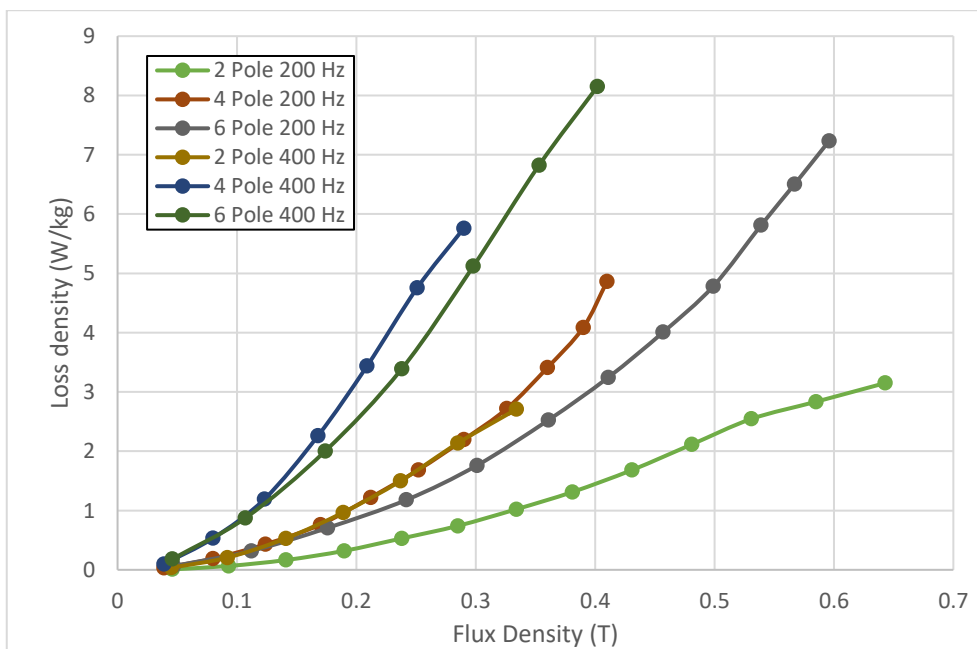


Figure 4.15: Specific core loss of the stator under test measured with the new core loss tester with 2-pole, 4-pole and 6-pole connection of the excitation coil winding at 200 Hz and 400 Hz frequency

4.3.2.3 Specific Loss Comparison with Epstein Frame Measurement

The new core loss tester measures the core loss under the influence of both pulsating and rotational excitation. The specific core loss measured using the new core loss tester were compared with the specific core loss measured by standard testers for pulsating core loss measurement like the Epstein frame. The comparison for a 2-pole connection at different frequencies is as shown in Figure 4.16.

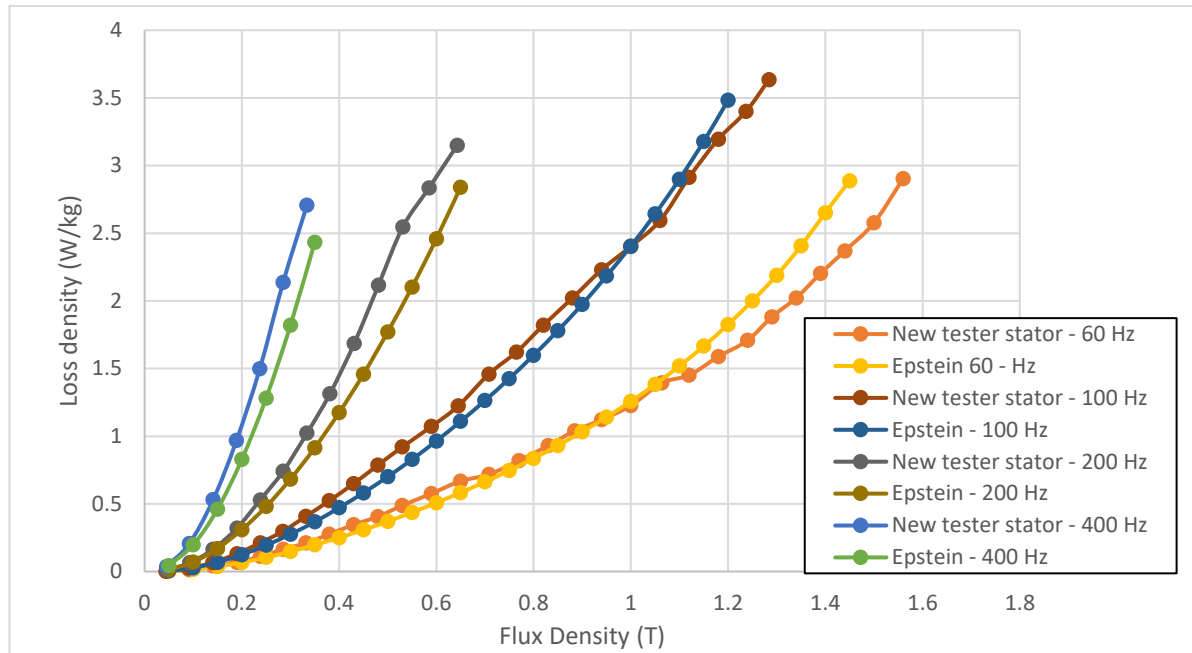


Figure 4.16: Comparison of the specific core loss of the stator measured with the new tester with 2-pole connection and the Epstein frame at 60 Hz, 100 Hz, 200 Hz and 400 Hz

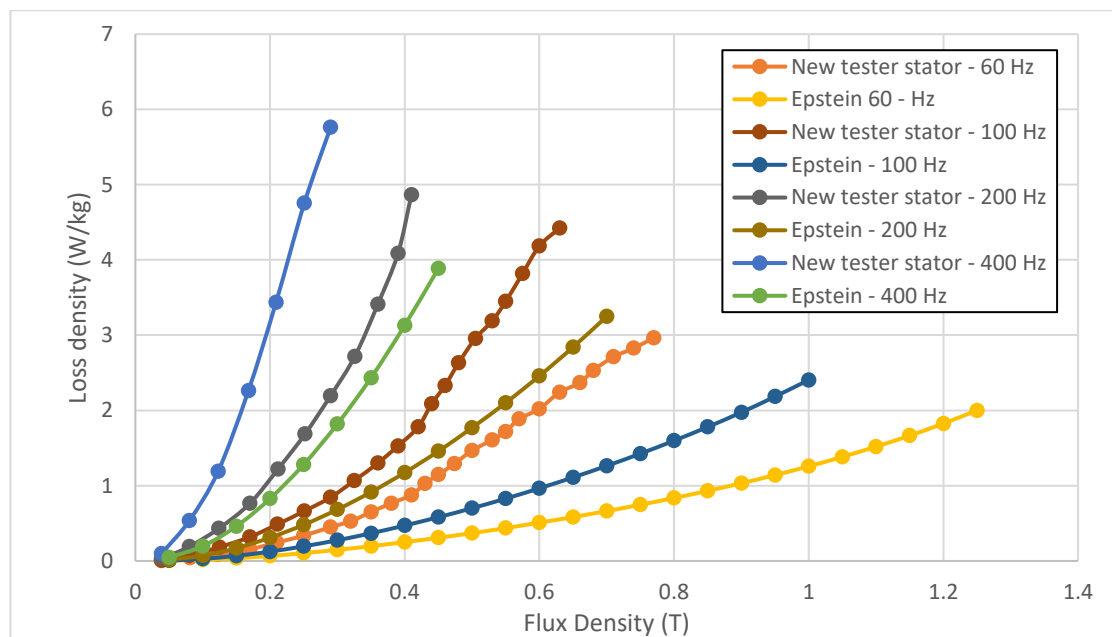


Figure 4.17: Comparison of the specific core loss of the stator measured with the new tester with 4-pole connection and the Epstein frame at 60 Hz, 100 Hz, 200 Hz and 400 Hz

Figure 4.17 and Figure 4.18 shows the comparison for the 4-pole and 6-pole connections respectively. The 2-pole connection gives flux distribution, which is nearly equal to pulsating flux distribution, as there will be only two major rotational zones available in the stator at a time. This results in similar specific core loss in the measurements with the new tester and the Epstein frame, which can be seen in Figure 4.16. For the 4-pole and 6-pole connections the specific core losses measured using the new tester are significantly higher compared to the Epstein frame specific loss measurement for the same material.

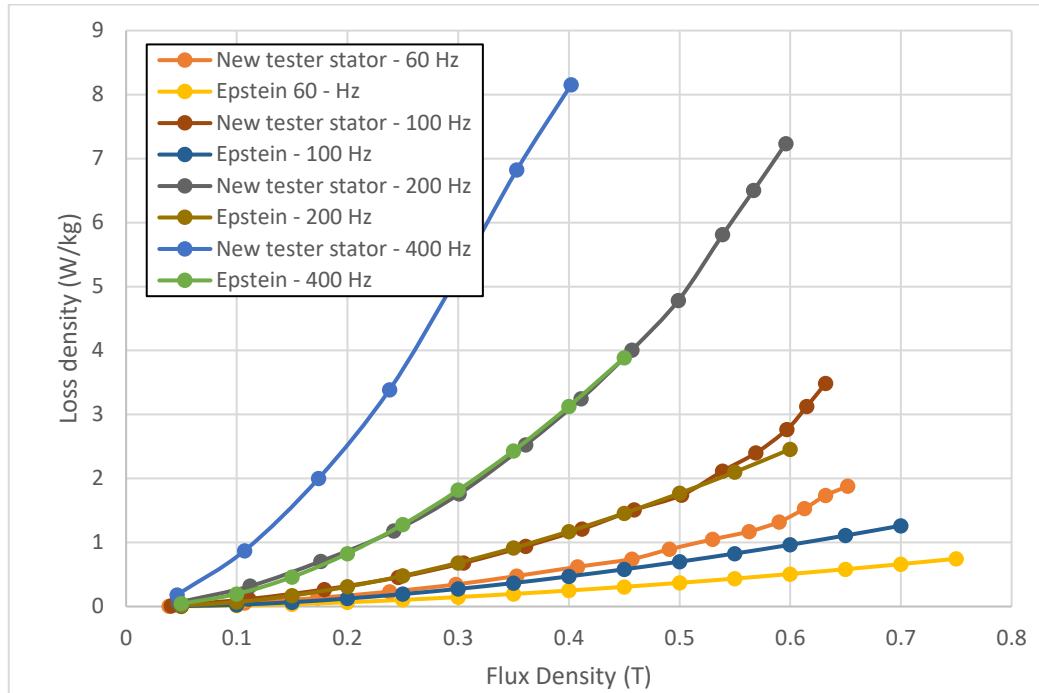


Figure 4.18: Comparison of the specific core loss of the stator measured with the new tester with 6-pole connection and the Epstein frame at 60 Hz, 100 Hz, 200 Hz and 400 Hz

Table 4.1 shows the comparison of total core loss of the tester and the stator measured by the new tester with the calculated total core loss of the Epstein frame using the specific core loss of Epstein frame for the tester and the stator material. The comparison shows that the total core loss at 60 Hz excitation with the 4-pole connection measured by the new tester is 72.4 % higher compared to the Epstein frame losses. The 2-pole connection gives the lowest difference in total core loss measurement between the new tester and the Epstein frame as discussed earlier. The reference quantity in the comparison is the tester peak flux density.

Table 4.1: Core loss comparison between the new tester and the Epstein frame

| Connection | Frequency (Hz) | Flux Density (T) | New Tester Loss ¹ (W) | Epstein Loss ² (W) | Percentage Difference |
|------------|----------------|------------------|----------------------------------|-------------------------------|-----------------------|
| 2 – Pole | 60 | 1 | 26.8 | 21.1 | 27.1 |
| | 100 | 1 | 50.0 | 40.7 | 22.8 |
| | 200 | 0.55 | 49.0 | 36.3 | 35.1 |
| | 400 | 0.35 | 54.89 | 42.7 | 28.4 |
| 4 - Pole | 60 | 1 | 36.3 | 21.1 | 72.4 |
| | 100 | 1 | 70.7 | 40.7 | 73.6 |
| | 200 | 0.55 | 75.0 | 36.3 | 106.8 |
| | 400 | 0.35 | 89.3 | 42.7 | 109.1 |
| 6 - Pole | 60 | 0.75 | 28.3 | 16.2 | 74.6 |
| | 100 | 0.7 | 51.3 | 21.6 | 138.1 |
| | 200 | 0.55 | 93.6 | 36.3 | 158.2 |
| | 400 | 0.35 | 116.3 | 42.7 | 172.2 |

¹Total core loss consisting of the tester and the stator measured by the new tester

²Total core loss of the Epstein frame calculated from the specific core loss of the Epstein frame measurement for tester and stator material

4.4 Comparison of Experimental Results, FE Simulation and Analytical Calculation

Table 4.2 gives the comparison of the total core losses observed from Finite Element (FE) simulation, analytical core loss calculation performed according to chapter 2 and the experimental core loss measured by the new tester. The reference quantity for the comparison is the peak tester flux density. The comparison shows that the core loss measured by the new tester is 35.4 percent and 38.1 percent higher than core loss calculated by finite element simulation at peak flux density of 1T in the tester with the 4-pole connection and 60 Hz and 100 Hz excitations respectively. Similarly, for the 6-pole connection and 0.45 T flux density, the difference in the core loss is 24.2 percent and 26.4 percent with 60 Hz and 100 Hz excitations respectively.

Table 4.2: Core loss comparison among FE simulation, analytical calculation and experimental results

| Total Core Loss (W) | | | | | | |
|----------------------------|-----------------------|-------------------------|----------------|-----------------------|-------------------------|--|
| Connection | Frequency (Hz) | Flux Density (T) | FEA (W) | Analytical (W) | Experimental (W) | Percentage Difference¹ |
| 4 – Pole | 60 | 1 | 26.8 | 31.6 | 36.3 | 35.8 |
| | 100 | 1 | 51.2 | 61.5 | 70.7 | 38.1 |
| 6 – Pole | 60 | 0.45 | 10.7 | 10.7 | 13.3 | 24.2 |
| | 100 | 0.45 | 20.3 | 20.4 | 25.7 | 26.4 |

¹Percentage difference between the core loss obtained from the Finite Element simulation and the experimental results

The large difference between the FE simulated core loss and experimental results is due to the fact that the core loss data used in FE simulation is the pulsating core loss data obtained from Epstein frame test using commercially available core loss tester or from the steel suppliers. The experimentally measured core loss is measured under the influence of rotational excitation.

Another factor affecting the experimentally measured core loss is the effect of mechanical processes performed on the steel sheets for the tester and the stator manufacturing like punching, laser cutting, stack pressing, etc. Epstein frame uses steel strips for core loss measurement, which is not affected by the mechanical processes. These mechanical processes degrades the magnetic properties of the electrical steel and increases the core loss as explained in chapter 2.

The complete comparison of the core loss calculation and experimental measurements is not presented due to the limitation of the experimental system to perform core loss measurement at higher frequency and higher flux density.

4.5 Summary

The core loss calibration of the tester was performed. The tester to stator flux density ratio was defined by performing various tests using the new tester. The validity of the experimental results was tested by comparing the experimental waveforms with the simulated waveforms from chapter 2. Comparison of the core loss measurements have been performed

on an induction machine stator using the newly prototyped core loss tester at various frequencies of 60, 100, 200 and 400 Hz with different number of pole combinations like 2, 4, and 6-pole. The measured core loss was separated between the tester and the stator under test using the method explained in chapter 3.

A comparative study of the core loss for different excitation frequencies and the number of pole was performed. The number of poles of the excitation winding is found to have an effect on the measured core loss. The difference between the core loss measurement with the pulsating excitation and the rotational excitation have been studied and the percentage difference between both of them have been found. The mechanical processes performed on the electrical steel for electrical machine manufacturing degrades the magnetic properties of the steel, especially at higher frequency and higher flux density and this was evident from the comparison of the experimental results with results from FE simulation.

5. Conclusions and Future Work

5.1 Conclusions

Methods and devices used for the measurement of pulsating and rotational core losses have been reviewed. The watt-metric method is found to be the most convenient and reliable method, which is used in this work. Techniques for measuring the magnetic flux density (\mathbf{B}) are presented.

A novel design for a core loss tester for the core loss estimation in the assembled stator stacks is analyzed, which allows core loss estimation in the stator prior to final machine assembly. The new tester gives a researcher the opportunity to improve an understanding of the effect of non-uniformity of flux density distribution on the core losses. The applied field magnitude, signal shape, the number of poles and the excitation frequency can be easily modified and controlled using the new core loss tester, making the developed tester highly flexible. This tester is capable of performing core loss measurements under the influence of both sinusoidal and non-sinusoidal magnetization. In addition, due to the toroidal structure of the new core loss tester, it can be used to study the impact of short pitching in induction and wound rotor synchronous machines and the magnet pole arc variation in permanent magnet machines on the core loss.

Extensive simulations using the different excitation frequencies and number of pole combinations of the excitation winding are performed. The new tester generates a rotating radial flux distribution in the stator core under test, which is similar to the flux distribution inside the actual machine while rotating.

Analytical core loss calculations were performed using the magnetic and dimensional data from the simulation. An equivalent magnetic flux density and frequency based core loss calculation algorithm developed by the other researchers in the laboratory was used for this purpose. The analytical results shows good correlation with the simulated core loss. The new tester proves use of watt-metric method for rotational core loss measurement.

The new tester is prototyped and operated successfully. The results from the tester were validated by comparing the results from FE simulation. Measurements were carried out on an induction machine stator made up of M36 gauge 29 silicon steel laminations with 36 slots, 125 mm stack length and 109 mm inner diameter. The calibration of the new tester was carried out using the ring tester to separate the tester core losses from the total measured losses. The tester to stator flux density ratio was also calibrated in order to perform the stator core loss measurement without winding any sensor coils on the stator.

The basic core loss measurements show that obtaining the rotational core losses from the sum of pulsating losses is not accurate. The difference between the experimentally measured and simulated core losses is mainly attributed to the effect of the asymmetry in the magnetic flux distribution in the stator and the tester core.

A comprehensive study has been conducted to understand the influence of the rotating magnetic fields and the number of poles on the core loss estimation. The investigation was carried out by comparing the experimental results with the simulation and analytical calculations. The comparison shows that the experimental core losses are 36% higher compared to the simulated core losses in a 4-pole connection and 60 Hz excitation frequency. This difference in the core losses is due to the use of pulsating core loss data supplied by steel manufacturers for the simulation.

The core losses measured by the new tester are compared with the core loss measured by the Epstein frame. It is found out from the comparison that the mechanical processes performed on the electrical steel like punching, laser cutting and stack pressing for manufacturing of the stators degrades the magnetic properties and increases core losses of the steel. Since the Epstein frame uses simple strips to measure core losses, the core losses measured by the new tester were 72% higher compared to the core losses measured by the Epstein frame.

5.2 Limitations

In this section some of the limitations of the new tester are provided:

- The tester and the stator needs to be aligned properly in order to perform accurate core loss measurement. This alignment includes the air gap and the vertical alignment between the slack lengths of the tester and the stator.
- The core loss of the tester needs to be calibrated accurately for accurate loss separation between the tester and the stator.
- The ratio of the tester to stator flux density needs to be defined accurately by performing multiple tests with the tester and multiple stators to perform the core loss measurement without using the stator sensor coil.
- The setup requires adequate cooling to perform core loss measurement at higher frequency and higher flux density.

- Linear power amplifier current capacity limits the highest achievable flux density to 0.6 T at 200 Hz and 0.35 T at 400 Hz frequency.

5.3 Future Work

This section proposes a few future works for the new tester:

- The utility of the developed tester can be extended for non-sinusoidal measurements as explained in section 2.4.2.
- Development of an accurate lumped parameter mathematical model which will be able to verify the simulation results in terms of magnetic flux density, magnetic field intensity etc.
- To prepare thermal model of the tester for the hot spot study and the effect of core loss on the temperature of the various parts of the stator core.
- Characterization of the core losses of the tester using the proposed method in section 4.1 for accurate core loss separation between the tester and the stator.
- Linear amplifiers capable of delivering high current at high frequency is required for performing tests at high frequency and high flux density.
- Simulations can be performed using the rotational magnetic data instead of currently used pulsating magnetic data.
- The same concept can be extended for core loss estimation in the rotor by shifting the excitation windings to the stator.
- The use of the new tester for Soft Magnetic Composite (SMC) materials can be explored, as there is very little information available about the magnetic properties of the SMC materials.

5.4 Applications

This section presents some applications of the new core loss tester:

- Core loss estimation in the stator cores during electrical machine manufacturing before final machine assembly.
- Characterization of the stator magnetic properties for using in finite element (FE) simulations.
- To study the effect of short pitching, magnet pole arc variation and number of poles on the core loss of the stator and rotor.

- The core loss estimation of the stator and rotor made using Soft Magnetic Composite (SMC) materials.

References

- [1] "Electric Machines," [Online]. Available: <https://www.energy.gov/eere/amo/electric-machines>.
- [2] G. A. Mckoy, T. Litman and J. G. Douglass, Energy-Efficient Electric Motor Selection Handbook Review 3, Washington State Energy Office, January 1993.
- [3] G. Seggewiss, J. Dai and M. Fanslow, "Synchronous Motors on Grinding Mills: The Different Excitation Types and Resulting Performance Characteristics with VFD Control for New or Retrofit Installations," *IEEE Industry Applications Magazine*, vol. 21, no. 6, pp. 60-67, Nov.-Dec. 2015.
- [4] A. Boglietti, A. Cavagnino, D. M. Ionel, M. Popescu, D. A. Staton and S. Vaschetto, "A General Model to Predict the Iron Losses in PWM Inverter-Fed Induction Motors," *IEEE Transactions on Industry Applications*, vol. 46, no. 5, pp. 1882-1890, Sept.-Oct. 2010.
- [5] J. Gieras, "New applications of synchronous generators," *Przegląd Elektrotechniczny (Electrotechnical Review)*, vol. 88, no. 9a, pp. 150-157, 2012.
- [6] ASTM A343 / A343M-14, *Standard Test Method for Alternating-Current Magnetic Properties of Materials at Power Frequencies Using Wattmeter-Ammeter-Voltmeter Method and 25-cm Epstein Test Frame*, West Conshohocken, PA: ASTM International, 2019.
- [7] ASTM A348 / A348M-05, *Standard Test Method for Alternating Current Magnetic Properties of Materials Using the Wattmeter-Ammeter-Voltmeter Method, 100 to 10 000 Hz and 25-cm Epstein Frame*, West Conshohocken, PA: ASTM International, 2015.
- [8] ASTM A927 / A927M-18, *Standard Test Method for Alternating-Current Magnetic Properties of Toroidal Core Specimens Using the Voltmeter-Ammeter-Wattmeter Method*, West Conshohocken, PA: ASTM International, 2018.
- [9] ASTM A804 / A804M-04, *Standard Test Methods for Alternating-Current Magnetic Properties of Materials at Power Frequencies Using Sheet-Type Test Specimens*, West Conshohocken, PA: ASTM International, 2015.
- [10] L. T. Mthombeni and P. Pillay, "Core losses in motor laminations exposed to high-frequency or nonsinusoidal excitation," *IEEE Transactions on Industry Applications*, vol. 40, no. 5, pp. 1325-1332, Sept.-Oct. 2004.

- [11] J. Sievert, H. Ahlers, M. Birkfeld, B. Cornut, F. Fiorillo, K. A. Hempel, T. Kochmann, A. Kedous-Lebouc, T. Meydan, A. Moses and A. M. Rietto, "European intercomparison of measurements of rotational power loss in electrical sheet steel," *Journal of Magnetism and Magnetic Materials*, vol. 160, pp. 115-118, 1996.
- [12] H. Pfutzner, E. Mulasalihovic, H. Yamaguchi, D. Sabic, G. Shilyashki and F. Hofbauer, "Rotational Magnetization in Transformer Cores—A Review," *IEEE Transactions on Magnetics*, vol. 47, no. 11, pp. 4523-4533, Nov. 2011.
- [13] C. Ragusa, S. Zurek, C. Appino and A. J. Moses, "An intercomparison of rotational loss measurements in non-oriented Fe–Si alloys," *Journal of Magnetism and Magnetic Materials*, vol. 320, no. 20, pp. e623-e626, 2008.
- [14] S. Zurek and T. Meydan, "Errors in the power loss measured in clockwise and anticlockwise rotational magnetisation. Part 1: Mathematical study," *IEE Proceedings - Science, Measurement and Technology*, vol. 153, no. 4, pp. 147-151, 7 July 2006.
- [15] M. Jesenik, V. Goričan, M. Trlep, A. Hamler and B. Štumberger, "Eddy Current Effects in the Sample of 2D R.R.S.S.T. and in the Sample of 2D S.R.S.S.T.," in *Computer Engineering in Applied Electromagnetism*, Dordrecht, Springer, 2005, pp. 297-300.
- [16] J. Wanjiku and P. Pillay, "Design Considerations of 2-D Magnetizers for High Flux Density Measurements," *IEEE Transactions on Industry Applications*, vol. 51, no. 5, pp. 3629-3638, Sept.-Oct. 2015.
- [17] N. Alatawneh and P. Pillay, "Design of a Novel Test Fixture to Measure Rotational Core Losses in Machine Laminations," *IEEE Transactions on Industry Applications*, vol. 48, no. 5, pp. 1467-1477, Sept.-Oct. 2012.
- [18] A. M. El-Refaie, "Motors/generators for traction/propulsion applications: A review," *IEEE Vehicular Technology Magazine*, vol. 8, no. 1, pp. 90-99, March 2013..
- [19] A. Krings, M. Cossale, J. Soulard, A. Boglietti and A. Cavagnino, "Manufacturing influence on the magnetic properties and iron losses in cobalt-iron stator cores for electrical machines," in *IEEE Energy Conversion Congress and Exposition (ECCE)*, Pittsburgh, PA, 2014.
- [20] A. Boglietti, A. Cavagnino, M. Lazzari and M. Pastorelli, "Effects of punch process on the magnetic and energetic properties of soft magnetic material," in *IEEE International Electric Machines and Drives Conference*, Cambridge, MA, USA, 2001.

- [21] S. Elfgen, S. Steentjes, S. Böhmer, D. Franck and K. Hameyer, "Influences of Material Degradation Due to Laser Cutting on the Operating Behavior of PMSM Using a Continuous Local Material Model," *IEEE Transactions on Industry Applications*, vol. 53, no. 3, pp. 1978-1984, May-June 2017.
- [22] H. A. Weiss, P. Tröber, R. Golle, W. Volk, S. Steentjes, N. Leuning, S. Elfgen and K. Hameyer, "Impact of Punching Parameter Variations on Magnetic Properties of Nongrain-Oriented Electrical Steel," *IEEE Transactions on Industry Applications*, vol. 54, no. 6, pp. 5869-5878, Nov.-Dec. 2018.
- [23] L. Masisi, M. Ibrahim, J. Wanjiku, A. M. Aljehaimi and P. Pillay, "The Effect of Two- and Three-Level Inverters on the Core Loss of a Synchronous Reluctance Machine (SynRM)," *IEEE Transactions on Industry Applications*, vol. 52, no. 5, pp. 3805-3813, Sept.-Oct. 2016.
- [24] M. Oka, T. Ogasawara, N. Kawano and M. Enokizono, "Estimation of Suppressed Iron Loss by Stress-Relief Annealing in an Actual Induction Motor Stator Core by Using the Excitation Inner Core Method," *IEEE Transactions on Magnetics*, vol. 50, no. 11, pp. 1-4, Nov. 2014.
- [25] T. Okubo, G. Shilyashki, H. Pfützner, A. Kenov and Y. Oda, "Can Circular Rotational Losses of Non-Oriented Soft Magnetic Materials Be Estimated From Alternating Losses," *IEEE Transactions on Magnetics*, vol. 54, no. 12, pp. 1-6, Dec. 2018.
- [26] N. Stranges and R. D. Findlay, "Methods for predicting rotational iron losses in three phase induction motor stators," *IEEE Transactions on Magnetics*, vol. 36, no. 5, pp. 3112-3114, Sept 2000.
- [27] S. Nazrulla, E. G. Strangas, J. S. Agapiou and T. A. Perry, "A Device for the Study of Electrical Steel Losses in Stator Lamination Stacks," *IEEE Transactions on Industrial Electronics*, vol. 61, no. 5, pp. 2217-2224, May 2014.
- [28] D. Schmitz, N. Sadowski, S. L. Nau, N. J. Batistela and J. P. A. Bastos, "Three-Phase Electromagnetic Device for the Evaluation of the Magnetic Losses in Electric Motors," *IEEE Transactions on Energy Conversion*, vol. 30, no. 2, pp. 515-521, June 2015.
- [29] A. Takbash, M. Ibrahim, L. Masisi and P. Pillay, "Core Loss Calculation in a Variable Flux Permanent Magnet Machine for Electrified Transportation," *IEEE Transactions on Transportation Electrification*, vol. 4, no. 4, pp. 857-866, Dec. 2018.

- [30] N. Stranges, *An Investigation of Iron Losses Due to Rotating Flux in Three Phase Induction Motor Cores*, Hamilton: PhD, McMaster University, 2000.
- [31] J. C. Akiror, A. Merkhouf, C. Hudon and P. Pillay, "Consideration of Design and Operation on Rotational Flux Density Distributions in Hydrogenerator Stators," *IEEE Transactions on Energy Conversion*, vol. 30, no. 4, pp. 1585-1594, Dec. 2015.

Appendix

Appendix A: MATLAB Simulink[®] schematic for generation and sensing of the required waveforms

The Figure in appendix shows the MATLAB Simulink[®] schematic used in this work for generation and sensing of all the waveforms explained in the above chapters. The flexibility in terms of the magnitude and the frequency of the generated waveforms can be achieved using this schematic. The common gain control and protection is provided for both the amplifiers in order to make the gain of both the amplifiers same at each testing point.

